Low Thrust Trajectory Optimization in the Saturn-Titan System

by

Anirudh Etagi

B.Tech., People's Education Society University, 2023

A thesis submitted to the

Faculty of the Graduate School of the

University of Colorado in partial fulfillment

of the requirements for the degree of

Master of Science

Department of Aerospace Engineering Sciences

2025

Committee Members:

Prof. Natasha Bosanac, Chair

Prof. Daniel Scheeres

Prof. Jay McMahon

Etagi, Anirudh (MS., Aerospace Engineering Sciences)

Low Thrust Trajectory Optimization in the Saturn-Titan System

Thesis directed by Prof. Natasha Bosanac

The growing interest in missions to the moons of Jupiter and Saturn motivates trajectory optimization within these systems. This thesis focuses on the computation of propellant mass optimal trajectories for spacecraft with low thrust propulsive systems in the Saturn-Titan system. The Circular Restricted Three Body Problem (CR3BP) is used to describe the dynamical environment. The equations are modified to incorporate low thrust contributions. The method to generate an initial guess trajectory is defined. Trajectory optimization using primer vector theory is used along with multiple shooting to generate the required transfers. Necessary conditions are derived for the chosen dynamical system. Propellant mass optimal transfers to vertical and halo target orbits are computed to achieve coverage of the polar regions of Titan. The resultant halo orbit transfer is then utilized to generate transfers to a nearby NRHO orbit for closer approaches to the south polar region.

Dedication

I would like to dedicate this thesis to my family, who have helped and supported me for the longest time, and to my friends who kept me sane during the sleepless nights.

Acknowledgements

I would like to thank my family for all of their help and for supporting me in my decisions and goals. To my friends, thank you for helping me with all the spirals - mental as well as trajectories. I would like to thank all the professors and mentors at CU Boulder that have helped and inspired me along this journey. In particular, I would like to thank Prof. Bosanac for all the guidance and knowledge over the course of this thesis.

Contents

Chapter

Tables

Table

Figures

Figure

Chapter 1

Introduction

1.1 Motivation

The launch of the Europa Clipper mission marks a new entry in the growing list of missions aimed at exploring the outer regions of our solar system. Several missions in recent years have been developed and launched, with aims of exploring Saturnian and Jovian environments. Study of Titan's methane lakes provide an opportunity to study the development of liquids on celestial bodies. In addition, missions aimed at studying the polar methane lakes could also be repurposed to perform other studies, such as gravity field studies and polar weather analysis. The surge in interest in solar system exploration calls for further analysis and development of trajectories within planetary systems.

1.2 Optimal Trajectories

Optimization is a vital aspect of the trajectory design process, especially having to cover a large distance as in the case of the Saturnian system. Optimization is essential in order to extend the operational lifetime of any mission, due to the limited amount of propellant that can be carried. The mathematics at the core of optimal control theory allow us to obtain mathematical conditions which can guarantee optimality. Optimization is an extremely broad field, with several different approaches possible. However, these approaches can be broadly categorized into two types : direct and indirect.

Direct optimization relies on discretizing an initial solution into nodes. A performance metric

is minimized by using nonlinear programming methods in order to solve for a set of control variables. A significant advantage of direct methods is that they are extremely robust to the initial guess used. However, the lack of mathematical conditions to ensure optimality results in a lack of optimality guarantee for any solution obtained [4].

Indirect methods on the other hand, work by defining a boundary value problem and cost function. The cost function is a metric of performance to be optimized. This involves the use of adjoint variables, dynamic Lagrange multipliers which need to be solved for. In addition, necessary conditions are derived which, when satisfied can ensure at least locally optimal solutions. The biggest advantage of indirect approaches is that, upon satisfying all necessary and optimality conditions, the solution obtained is guaranteed to be locally optimal. However, the solution is extremely sensitive to the quality of the initial guess. Any solution to be achieved must lie satisfactorily close to the initial guess utilized. Due to the guarantees of optimality, this thesis utilizes an indirect optimization approach.

Indirect optimization methods utilize optimal control theory, which utilizes Hamiltonian mechanics in order to define necessary conditions, which must be satisfied to achieve an optimal solution. D.F Lawden was instrumental in the development of optimal control theory as applied to spacecraft trajectory optimization[8]. He developed the 'Primer Vector Theory' approach to optimization which is commonly used to generate trajectories with a goal to minimize aspects such as propellant usage or to achieve minimum time of flight trajectories. Lawden's work has been used extensively in order to optimize spacecraft trajectories with respect to different metrics, such as time of flight or propellant usage[17, 14, 12]

A vital aspect of interplanetary exploration is the need to minimize the propellant usage. With interplanetary missions, one of the most important aspect is to make the most of every drop of propellant available. This is because of the lack of easy refueling options available. If an interplanetary mission runs out of propellant, there is nothing that can be done to restore the spacecraft Thus, being able to generate efficient and propellant mass optimal trajectories is a vital aspect of the trajectory design procedure.

Indirect optimization can also incorporate practical constraints, such as upper limits on the amount of thrust which the propulsive system in question can generate. In addition, constraints can also be enforced to ensure the trajectory is completed within a specific amount of time.

1.3 Thesis Overview

The goal of this thesis is to generate optimal transfers from the vicinity of Saturn to selected libration point orbits in the vicinity of Titan, Saturn's largest moon. The structure of the thesis is described as follows

- Chapter 2 introduces the dynamical model used, the Circular Restricted Three Body Problem (CR3BP). Equations of motion are presented and fundamental solutions are described. The dynamical model is then modified to incorporate low thrust acceleration.
- Chapter 3 introduces the procedure used to correct trajectories.
- Chapter 4 describes the fundamentals of indirect optimization and optimal control theory for a general problem statement. Next, the optimizations procedure is applied to the defined dynamical model. Necessary conditions to ensure optimality are defined
- Chapter 5 details the specific approach used to generate propellant optimal trajectories, including the selection of the target orbits, the constraints to be enforced and the procedure detailing the selection of an initial guess trajectory.
- Chapter 6 details the resultant propellant mass optimal trajectories obtained. Analysis of the results is performed to gain insights into the solution space. The resultant halo orbit transfer is utilized to continue onto a transfer to a nearby NRHO orbit.
- Chapter 7 summarizes the findings of the thesis and future work is discussed

Chapter 2

Dynamical Model

2.1 Equations of Motion

The dynamical model used in this report is the Saturn-Titan Circular Restricted Three body problem. This model includes three bodies - Saturn, Titan and the spacecraft. P_1, P_2 and P_3 refer to Saturn, Titan, and the spacecraft with masses $\tilde{M}_1$, $\tilde{M}_2$ and $\tilde{M}_3$ respectively. $\tilde{M}_1$ is the largest of the three. The position and velocities of the bodies in the inertial frame are denoted by $\left(\tilde{X}_i, \quad \tilde{Y}_i, \quad \tilde{Z}_i, \quad \tilde{X}_i', \quad \tilde{Y}_i', \quad \tilde{Z}_i' \right) \forall i = 1, 2, 3$. Here, capital letters and $'$ indicate that the quantities are defined in an inertial frame and derivatives are computed with respect to time. $\tilde{}$ denotes that the quantities used are dimensional. The position vectors for each body $\mathrm{P_i}$ in the inertial frame is given by $\vec{\tilde{R}}_i = \tilde{X}_i\hat{X} + \tilde{Y}_i\hat{Y} + \tilde{Z}_i\hat{Z}$

The potential function for P_3 is a function of the distance of the spacecraft to P_1 and P_2 as follows

$$\tilde{U}_3 = \frac{\tilde{G}\tilde{M}_1}{\tilde{R}_{13}} + \frac{\tilde{G}\tilde{M}_2}{\tilde{R}_{23}} \tag{2.1}$$

$\tilde{R}_{13}$ and $\tilde{R}_{23}$ denote the distance of the spacecraft to the first and second primaries respectively and are given by

$$\tilde{R}_{13} = \sqrt{\left(\tilde{X}_3 - \tilde{X}_1\right)^2 + \left(\tilde{Y}_3 - \tilde{Y}_1\right)^2 + \left(\tilde{Z}_3 - \tilde{Z}_1\right)^2} \tag{2.2}$$

$$\tilde{R}_{23} = \sqrt{\left(\tilde{X}_3 - \tilde{X}_2\right)^2 + \left(\tilde{Y}_3 - \tilde{Y}_2\right)^2 + \left(\tilde{Z}_3 - \tilde{Z}_2\right)^2} \tag{2.3}$$

The acceleration acting on the spacecraft (body 3) is written as

$$\vec{\tilde{R}}_3'' = \bigtriangledown\tilde{U}_3 = \frac{\partial\tilde{U}_3}{\partial X_3}\hat{X} + \frac{\partial\tilde{U}_3}{\partial Y_3}\hat{Y} + \frac{\partial\tilde{U}_3}{\partial Z_3}\hat{Z} \tag{2.4}$$

where

$$\vec{\tilde{R}}_3'' = \tilde{X}_3''\hat{X} + \tilde{Y}_3''\hat{Y} + \tilde{Z}_3''\hat{Z} \tag{2.5}$$

Using Equations 2.2, 2.3 and 2.5, Equation 2.4 can then be written in scalar form as

$$\tilde{X}_3'' = -\frac{\tilde{G}\tilde{M}_1\left(\tilde{X} - \tilde{X}_1\right)}{\tilde{R}_{13}^3} - \frac{\tilde{G}\tilde{M}_2\left(\tilde{X} - \tilde{X}_2\right)}{\tilde{R}_{23}^3} \tag{2.6}$$

$$\tilde{Y}_3'' = -\frac{\tilde{G}\tilde{M}_1\left(\tilde{Y} - \tilde{Y}_1\right)}{\tilde{R}_{13}^3} - \frac{\tilde{G}\tilde{M}_2\left(\tilde{Y} - \tilde{Y}_2\right)}{\tilde{R}_{23}^3} \tag{2.7}$$

$$\tilde{Z}_3'' = -\frac{\tilde{G}\tilde{M}_1\left(\tilde{Z} - \tilde{Z}_1\right)}{\tilde{R}_{13}^3} - \frac{\tilde{G}\tilde{M}_2\left(\tilde{Z} - \tilde{Z}_2\right)}{\tilde{R}_{23}^3} \tag{2.8}$$

Next, the following assumptions are used to simplify the dynamical model:

- Each body is modeled as having constant mass and point mass gravity field.
- $\tilde{M}_3 << \tilde{M}_2 < \tilde{M}_1$ [20]
- Due to the mass of P_3 being negligible compared to the other two bodies, P_3 does not affect the paths of P_1 and P_2. Hence, the two primaries travel on conics about their mutual barycenter.
- P_1 and P_2 follow a circular path about their mutual barycenter [23].

In order to avoid discrepancies between the orders of magnitude between the length, mass and time quantities, we non-dimensionalize the obtained equations using certain characteristic quantities defined below.

A mass parameter μ is defined using the combined mass of the two primaries. The CR3BP system can be completely described using this single parameter. Changing the value of μ results in a different system. The value of μ ranges from 0 to 0.5

$$m^* = \tilde{M}_1 + \tilde{M}_2 \tag{2.9}$$

$$\mu = M_2 = \frac{\tilde{M}_2}{m^*} \tag{2.10}$$

$$1 - \mu = M_1 = \frac{\tilde{M}_1}{m^*} \tag{2.11}$$

Next, the characteristic length is defined using the distance between the two primaries. This is chosen to be the semi major axis of the Saturn-Titan two body system.

$$l^* = \tilde{a} \tag{2.12}$$

where $\tilde{a}$ is the semi major axis of the Saturn-Titan 2 Body system.

Finally, the characteristic time quantity is defined as

$$t^* = \sqrt{\frac{(l^*)^3}{\tilde{G}m^*}} \tag{2.13}$$

We define the non dimensional Gravitation constant G as follows

$$G = \frac{\tilde{G}m^* (t^*)^2}{(l^*)^3} = 1 \tag{2.14}$$

We non-dimensionalize the various quantities of our dynamical model as follows

$$X = \frac{\tilde{X}}{l^*} \tag{2.15}$$

$$Y = \frac{\tilde{Y}}{l^*} \tag{2.16}$$

$$Z = \frac{\tilde{Z}}{l^*} \tag{2.17}$$

$$R_{13} = \frac{\tilde{R}_{13}}{l^*} \tag{2.18}$$

$$R_{23} = \frac{\tilde{R}_{23}}{l^*} \tag{2.19}$$

$$t = \frac{\tau}{t^*} \tag{2.20}$$

Where, τ is the dimensional time quantity In addition, as the the primaries are considered to be in a conic path about their mutual barycenter, from the two body problem, we have

$$n = \sqrt{\frac{\mu_{2BP}}{a^3}} = 1 \tag{2.21}$$

Hence, using the nondimensionalized quantities defined above, Equations 2.40, 2.41 and 2.42 can be expressed using non dimensionalized quantities as

$$X'' = -\frac{(1-\mu)(X - X_1)}{R_{13}^3} - \frac{\mu (X - X_2)}{R_{23}^3} \tag{2.22}$$

$$Y'' = -\frac{(1-\mu)(Y-Y_1)}{R_{13}^3} - \frac{\mu(Y-Y_2)}{R_{23}^3} \tag{2.23}$$

$$Z'' = -\frac{(1-\mu)(Z-Z_1)}{R_{13}^3} - \frac{\mu(Z-Z_2)}{R_{23}^3} \tag{2.24}$$

The subscript 3 is dropped from all subsequent equations for the sake of convenience.

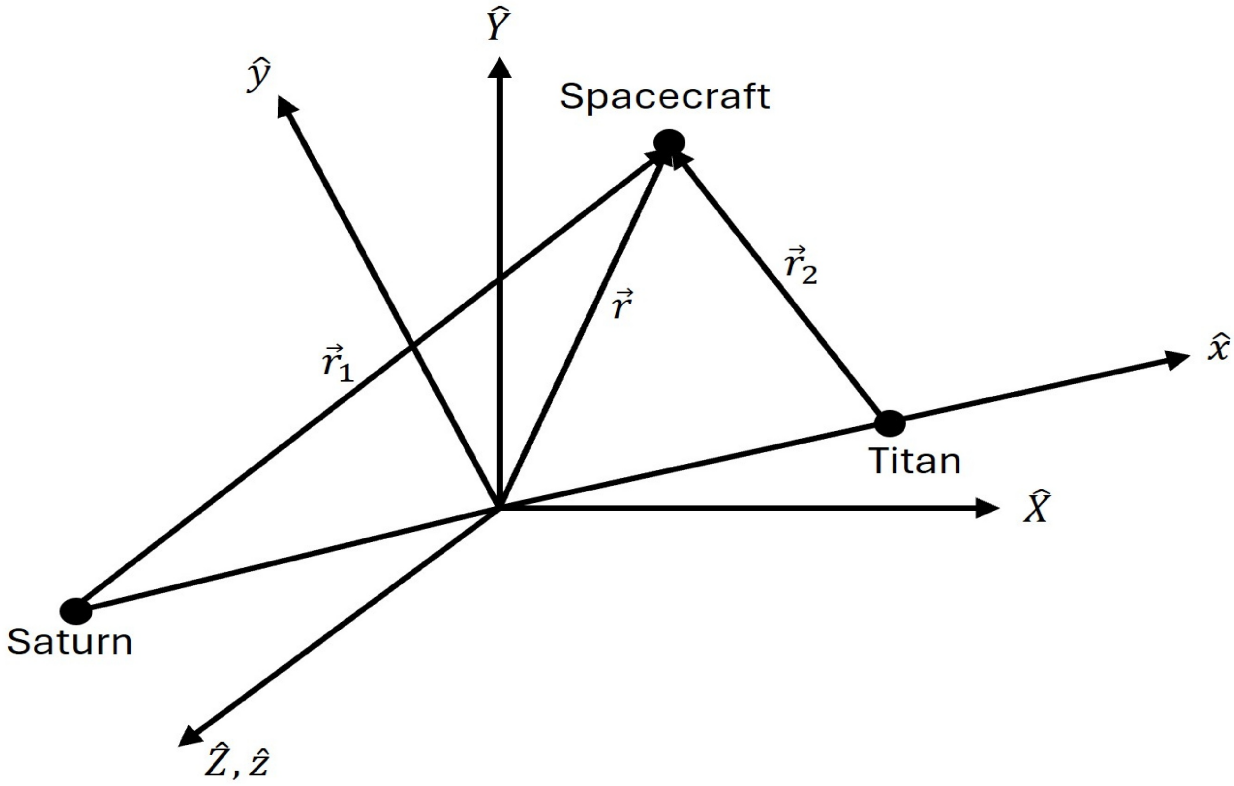

Figure 2.1: Rotating frame definition

Next, we define a rotating frame centered at the barycenter of the primaries as shown in Fig 2.1. In this frame, lower case letters and $\dot{}$ are used to indicate the rotating frame quantities and the rotating frame derivatives. The x axis of the rotating frame is defined from P_1 to P_2 as shown. The z axis coincides with the inertial frame Z axis and the y frame completes the right handed coordinate frame. The position vectors of the primaries from the origin of the system is defined as

$$\vec{r}_{1P} = x_1\hat{x} \tag{2.25}$$

$$\vec{r}_{2P} = x_2\hat{x} \tag{2.26}$$

The position of the center of mass of the primaries can be expressed as follows

$$0 = \frac{M_1 x_1 + M_2 x_2}{M_1 + M_2} \tag{2.27}$$

The rotating frame is defined in such a way so as to ensure that the distance between the primaries is unity. Thus, $\vec{r}_{P1} + \vec{r}_{P2} = 1$. Using this condition, the specific locations of the primaries can be determined as

$$x_1 = -\mu \tag{2.28}$$

$$x_2 = (1 - \mu) \tag{2.29}$$

The vectors $\vec{r}$, $\vec{r}_1$ and $\vec{r}_2$ denote the spacecraft position with respect to the barycenter and the two primaries. Hence, we can expand $\vec{r}$, $\vec{r}_1$ and $\vec{r}_2$ as follows

$$\vec{r} = x\hat{x} + y\hat{y} + z\hat{z} \tag{2.30}$$

$$\vec{r}_1 = (x + \mu)\,\hat{x} + y\hat{y} + z\hat{z} \tag{2.31}$$

$$\vec{r}_2 = (x - 1 + \mu)\,\hat{x} + y\hat{y} + z\hat{z} \tag{2.32}$$

The transformation between the inertial and rotating frame is as follows

$$\begin{bmatrix} x \\ y \\ z \end{bmatrix} = \begin{bmatrix} \cos(t) & \sin(t) & 0 \\ -\sin(t) & \cos(t) & 0 \\ 0 & 0 & 1 \end{bmatrix} \begin{bmatrix} X \\ Y \\ Z \end{bmatrix} \tag{2.33}$$

The angular velocity of the rotating frame with respect to the inertial frame is given as

$$\vec{\omega}_{R/I} = n\hat{z} = \hat{z} \tag{2.34}$$

The velocity of the spacecraft is written in rotating frame components as

$${}^{R}\vec{v}_1 = \dot{x}\hat{x} + \dot{y}\hat{y} + \dot{z}\hat{z} \tag{2.35}$$

The conversion between derivative terms between the inertial and rotating frame is given below using the transport theorem [15]

$$\frac{{}^{I}d\vec{r}}{dt} = \frac{{}^{R}d\vec{r}}{dt} + \vec{\omega}_{R/I} \times \vec{r} \tag{2.36}$$

$$\therefore \frac{^I d\vec{r}}{dt} = (\dot{x} - y)\,\hat{x} + (\dot{y} + x)\,\hat{y} + z\hat{z} \tag{2.37}$$

Similarly, the relation between inertial and rotating frame accelerations is expressed as

$$\frac{^I d\vec{v}}{dt} = \frac{^R d\vec{v}}{dt} + \vec{\omega}_{R/I} \times \vec{v} \tag{2.38}$$

$$\therefore \frac{^I d\vec{v}}{dt} = (\ddot{x} - 2\dot{y} - x)\,\hat{x} + (\ddot{y} + 2\dot{x} - y)\,\hat{y} + z\hat{z} \tag{2.39}$$

Using the above relations, the equations of motion are expressed in the rotating frame as

$$\ddot{x} = 2\dot{y} + x - \frac{(1-\mu)\,(x+\mu)}{r_1^3} - \frac{\mu\,(x-1+\mu)}{r_2^3} \tag{2.40}$$

$$\ddot{y} = -2\dot{x} + y - \frac{(1-\mu)\,y}{r_1^3} - \frac{\mu y}{r_2^3} \tag{2.41}$$

$$\ddot{z} = -\frac{(1-\mu)\,z}{r_1^3} - \frac{\mu z}{r_2^3} \tag{2.42}$$

2.1.1 Constants of Motion

There is a constant of motion for the CR3BP which is conserved under natural motion. The previously derived equations of motion are rewritten using derivatives of a potential function U* as follows

$$\ddot{x} - 2\dot{y} = \frac{\partial U^*}{\partial x} \tag{2.43}$$

$$\ddot{y} + 2\dot{x} = \frac{\partial U^*}{\partial y} \tag{2.44}$$

$$\ddot{z} = \frac{\partial U^*}{\partial z} \tag{2.45}$$

$$U^* = \frac{1}{2}\left(x^2 + y^2\right) + \frac{1-\mu}{r_1} + \frac{\mu}{r_2} \tag{2.46}$$

The dot product of the velocity vector and the acceleration vector results in the following equation

$$\dot{x}\ddot{x} + \dot{y}\ddot{y} + \dot{z}\ddot{z} = \frac{\partial U^*}{\partial x}\dot{x} + \frac{\partial U^*}{\partial y}\dot{y} + \frac{\partial U^*}{\partial z}\dot{z} \tag{2.47}$$

The right hand part of the equation is simply the total time derivative of U* Thus, integrating the above equation, we obtain

$$\frac{|\vec{v}|^2}{2} = U^* - \frac{C}{2} \tag{2.48}$$

$$C = 2U^* - |\vec{v}|^2 \tag{2.49}$$

C is the constant of integration and is named the Jacobi constant of the CR3BP. Thus, for a given natural trajectory, the Jacobi constant remains constant. For the same spacecraft position, the Jacobi constant increases with the decrease of $|\vec{v}|^2$.

2.1.2 Equilibrium Points

Although the equations of motion of the system are nonlinear, certain solutions can be obtained which lead to important results and impact the dynamics of the solution space. The equilibrium points are solutions where both velocity and acceleration are zero. These points can be determined by setting the first and second derivatives of the position components to zero. Thus, Equations 2.40, 2.41 and 2.42 are written as

$$0 = x - \frac{(1-\mu)(x+\mu)}{r_1^3} - \frac{\mu(x-1+\mu)}{r_2^3} = x\left(1 - \frac{1-\mu}{r_1^3} - \frac{\mu}{r_2^3}\right) + \mu(1-\mu)\left(\frac{1}{r_2^3} - \frac{1}{r_1^3}\right) \tag{2.50}$$

$$0 = y - \frac{(1-\mu)y}{r_1^3} - \frac{\mu y}{r_2^3} \tag{2.51}$$

$$0 = -\frac{(1-\mu)z}{r_1^3} - \frac{\mu z}{r_2^3} \tag{2.52}$$

First, we notice that any solution to these equations, must involve setting z equal to zero. Next, we observe that one way of satisfying the above equations is by setting y equal to zero. For this case, we have

$$0 = x - \frac{(1-\mu)(x+\mu)}{|x+\mu|^3} - \frac{\mu(x-1+\mu)}{|x-1+\mu|^3} \tag{2.53}$$

This equation becomes singular at the locations of the two primaries. This implies there exist equilibrium points at both sides of the primaries: one to the left of P_1, to the right of P_2 and one lying between P_1 and P_2. These solutions are termed L_3, L_2 and L_1, respectively. The equation must be solved using a root finding method such as the Newton-Raphson solver in order to find these three collinear equilibrium points, depending on the initial guess used. The Hill Restricted 3 body problem can be used to derive analytical solutions to the coordinates of the collinear equilibrium

points. These solutions can then be used in the CR3BP as an initial guess in order to locate specific equilibrium points effectively [16]

$$x_{L_1} = 1 - \left(\frac{\mu}{3}\right)^{\frac{1}{3}} \tag{2.54}$$

$$x_{L_2} = 1 + \left(\frac{\mu}{3}\right)^{\frac{1}{3}} \tag{2.55}$$

$$x_{L_3} = -1 \tag{2.56}$$

Next, we consider the case for which y$\neq$0. In order to satisfy Equation 2.50 and 2.51, the following equations must be satisfied

$$1 - \frac{(1-\mu)}{r_1^3} - \frac{\mu}{r_2^3} = 0 \tag{2.57}$$

$$\frac{1}{r_2^3} - \frac{1}{r_1^3} = 0 \tag{2.58}$$

The above equations are solved by $r_1 = r_2$. Using this condition, Equation 2.57 becomes

$$r_1^3 = 1 \tag{2.59}$$

Thus, the equilibrium points must satisfy $r_1 = r_2 = 1$. From this, the triangular equilibrium points are located at

$$x = \frac{1}{2} - \mu \tag{2.60}$$

$$y = \pm\frac{\sqrt{3}}{2} \tag{2.61}$$

The equilibrium points are shown for the Saturn-Titan System in Fig 2.2

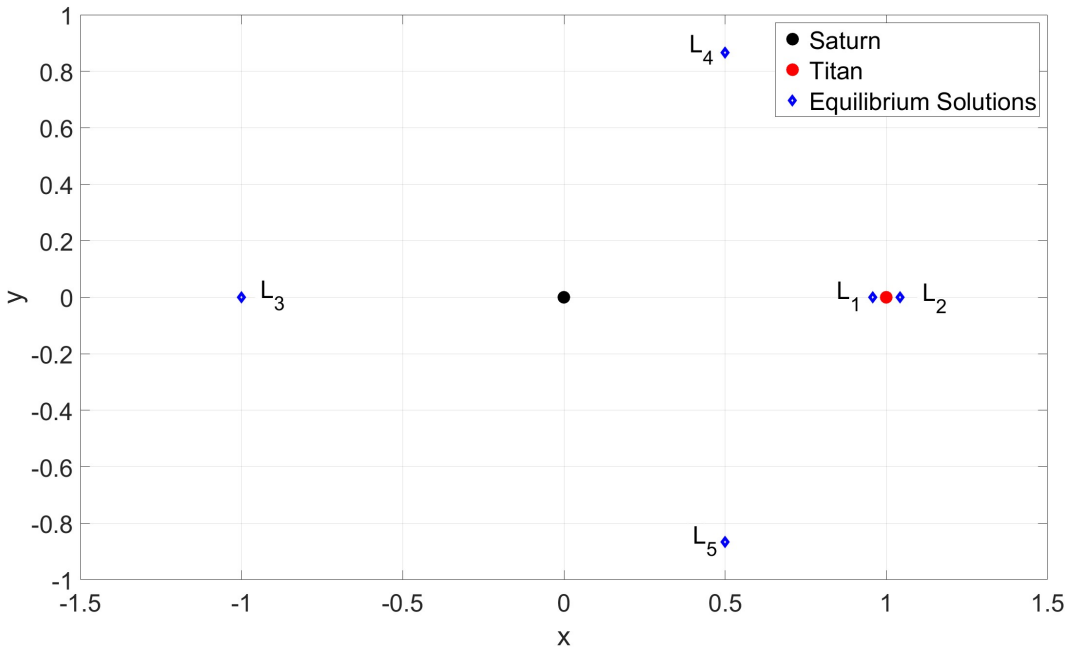

Figure 2.2: Equilibrium solutions for the Saturn-Titan CR3BP model

2.1.3 State transition Matrix

The state transition matrix is often used to study the sensitivity of a reference trajectory to perturbations. Given a reference state $\vec{x}_r$ and a state variation $\delta\vec{x}$ with respect to this reference state, the total state is given as follows

$$\vec{x} = \vec{x}_r + \delta\vec{x} \tag{2.62}$$

The reference state and state variation vectors both vary with time. The total state equations of motion is written as

$$\dot{\vec{x}} = \vec{f}\,(\vec{x}_r + \delta\vec{x}) = \dot{\vec{x}}_r + \delta\dot{\vec{x}}_r \tag{2.63}$$

Using a first order Taylor series expansion, the above expression is rewritten as

$$\dot{\vec{x}} = \dot{\vec{x}}_r + \delta\dot{\vec{x}}_r = \dot{\vec{x}}_r + \left.\frac{\partial\vec{f}}{\partial\vec{x}}\right|_r \delta\vec{x} \tag{2.64}$$

Hence, we can make the approximation

$$\delta\dot{\vec{x}} = \left.\frac{\partial\vec{f}}{\partial\vec{x}}\right|_r \delta\vec{x} \tag{2.65}$$

As this is a linear system of equations, a solution can be written as

$$\delta\vec{x}\,(t) = \phi\,(t, t_0)\,\delta\vec{x}\,(t_0) \tag{2.66}$$

where, $\phi\,(t, t_0)$ is defined as the state transition matrix (STM). The STM is a linear mapping to propagate the state deviations with respect to a certain reference trajectory. The differential equations governing the evolution of the STM is given as follows

$$\dot{\phi}\,(t, t_0) = [A]\,\phi\,(t, t_0) \tag{2.67}$$

where, $[A] = \left.\frac{\partial\vec{f}}{\partial\vec{x}}\right|_r$. The STM begins with an initial value of $\phi(t_0, t_0) = I_{n\times n}$. Utilizing the previously derived equations of motion for the CR3BP,

$$\vec{f} = \begin{bmatrix} \vec{v} \\ U_r^* + \vec{h}\,(\vec{v}) \end{bmatrix} \tag{2.68}$$

where, $U_r^* = \frac{\partial U^*}{\partial\vec{r}}$ and $\vec{h}\,(\vec{v}) = \begin{bmatrix} 2\dot{y} \\ -2\dot{x} \\ 0 \end{bmatrix}$ Thus, $[A]$ is defined as

$$[A] = \begin{bmatrix} 0_{3\times3} & I_{3\times3} \\ U_{rr}^* & \frac{\partial\vec{h}(\vec{v})}{\partial\vec{v}} \end{bmatrix} \tag{2.69}$$

where,

$$U_{rr}^* = \frac{\partial^2 U^*}{\partial\vec{r}^2} \tag{2.70}$$

$$\frac{\partial\vec{h}\,(\vec{v})}{\partial\vec{v}} = \begin{bmatrix} 0 & 2 & 0 \\ -2 & 0 & 0 \\ 0 & 0 & 0 \end{bmatrix} \tag{2.71}$$

2.2 Periodic Orbits

Periodic orbits in the CR3BP can be computed. These are trajectories which repeat in the rotating frame and exist in continuous families. The simplest family of periodic orbits which

exists in the CR3BP are the planar lyapunov orbits. These are the simplest to compute. The computation of Lyapnunov orbits is done by linearizing the equations of motion in the vicinity of the Lagrange points, using a first-order Taylor series expansion. This leads to the development of solutions for the in-plane variational equations. For specific locations in the vicinity of the Lagrange points, the solutions to the variational equations can be utilized to develop guesses for the corresponding velocities. Combined, these results can be used as an initial guess for a planar Lagrange point periodic orbit [20]. The initial guess must then be corrected in order to generate a repeating periodic orbit. This is done using the corrections procedure described in Chapter 3.1 This approach has been used to generate periodic orbits as seen in Fig 2.3. The larger the orbit, the more they deflect in the vicinity of the primary Titan.

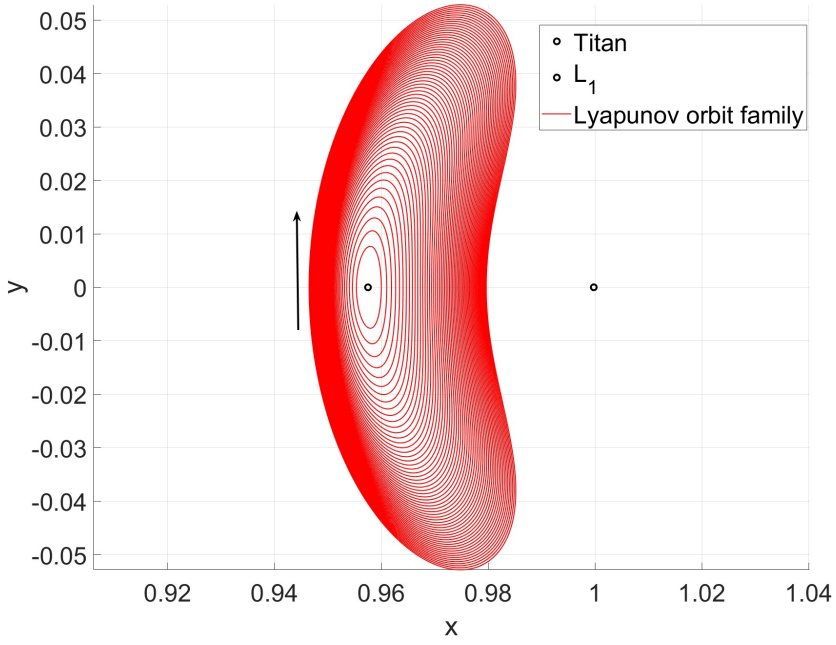

Figure 2.3: L_1 Lyapunov Orbit Family in the Saturn-Titan system

One example of spatial periodic orbits is the halo orbit family. These are categorized into northern and southern orbits. The two categories of halo orbits are symmetrical about the xy plane. The southern halo orbits reside under the xy plane for the majority of their orbit. Certain

members of the halo orbit families can have close approaches to the smaller primary. These close passes lead to the halo orbits being attractive target orbits for several mission. The L_1 northern halo orbit family is shown in Fig 2.4

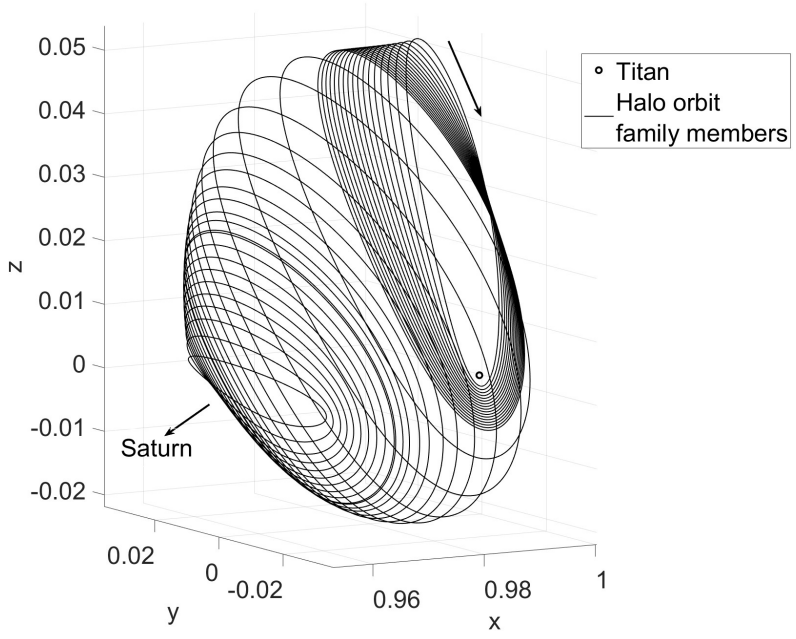

Figure 2.4: L_1 Northern halo orbit family

Several other types of periodic orbits, such as axial, vertical and butterfly orbits exist in the vicinity of the equilibrium points as well.

2.3 Orbit Stability and Bifurcations

Using the definition of the STM, the stability of a periodic orbit can be determined by examining the eigenvalues and eigenvectors of the Monodromy matrix. When considering periodic orbits, the Monodromy matrix is defined to be the STM after one full orbital period. Analysis of the eigenvectors can help us determine the existence of stable and unstable eigenspaces. Due to the symplectic quality of the Monodromy matrix, and the STM in general, the eigenvalues exist in reciprocal pairs [1]. Additionally, two of the 6 eigenvalues are equal to unity [1, 9]. The remaining

eigenvalues exist in pairs as follows

Given the non unity eigenvectors λ_1, λ_2, λ_3 and λ_4, the following relationships are found

$$\lambda_2 = \frac{1}{\lambda_1}, \quad \lambda_4 = \frac{1}{\lambda_3} \tag{2.72}$$

Stability indices are defined as the sum of the paired eigenvectors

$$s_1 = \lambda_1 + \lambda_2 \tag{2.73}$$

$$s_2 = \lambda_3 + \lambda_4 \tag{2.74}$$

The two indices can be utilized to assess the stability of the periodic orbit. Orbits corresponding to stability indices lying in the range [-2,2] are stable in the sense that, there exists stable and unstable eigenspaces. These eigenspaces can be used to compute invariant manifolds - stable and unstable. A spacecraft with a state on the stable manifold asymptotically approaches the periodic orbit, while one on the unstable manifold departs from the periodic orbit. These structures are often used in trajectory design processes.

It is found that, when a stability index equals 2, the periodic orbit in question defines the intersection of two distinct orbit families. Such intersections are termed as bifurcations. Interestingly, when a stability index equals -2, this is a special bifurcation where the reference trajectory has intersected with a member of a period doubling orbit family. This is a fundamental concept used in order to generate different types of period orbits. Beginning with a simple Lyapunov orbit family, bifurcations to halo and axial orbit families can be found [5]. Subsequently, the axial orbit family eventually bifurcates to vertical orbits. This is demonstrated in Figures 2.5 and 2.6. It can be seen that as we move along the members of an orbit family, we can observe the orbit where the family begins from. This orbit is also shared with a different orbit family and thus, represents the bifurcations predicted by the stability analysis. Fig 2.5 shows the blue orbit, where the Lyapunov orbit family bifurcates to give rise to the L_1 halo orbit family Similarly, in Fig 2.6, we first see the L_2 Lyapunov orbit family bifurcating to produce the axial orbit family. Next, we determine another bifurcation, where the vertical orbits can be obtained.

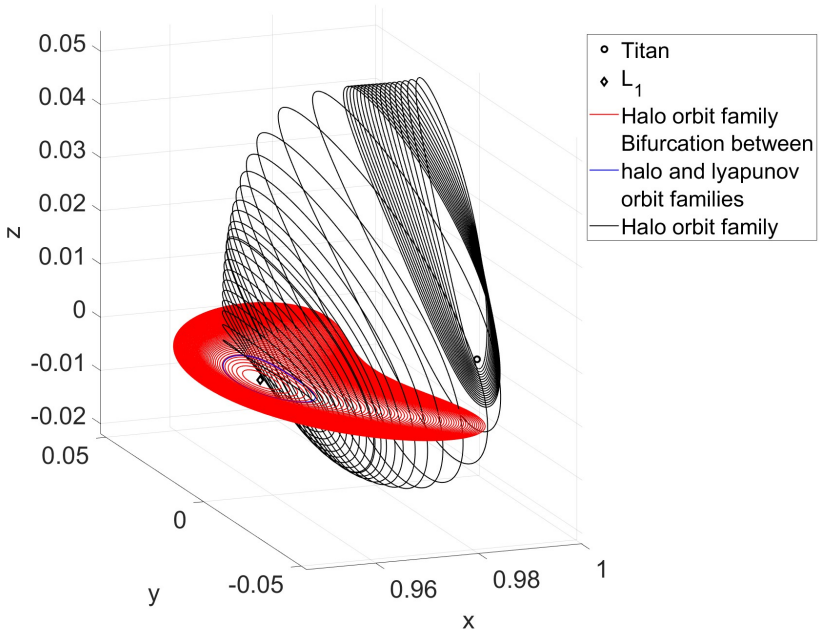

Figure 2.5: Bifurcation between L_1 lyapunov and halo orbit families

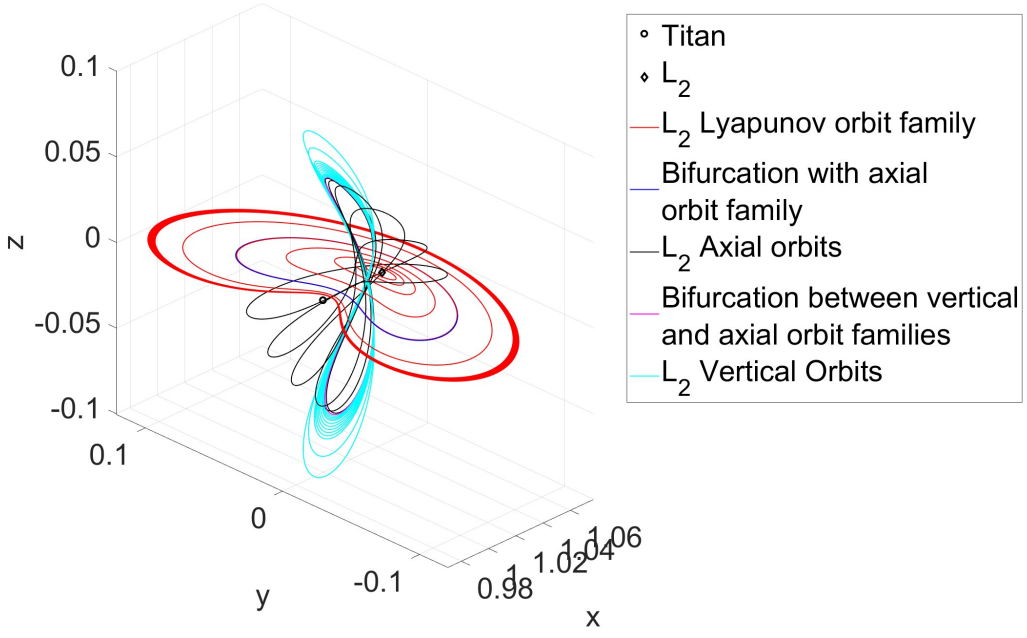

Figure 2.6: Bifurcations between various L_2 orbit families

2.4 Incorporating Low thrust into the CR3BP

The equations of motion can be perturbed by adding a disturbing acceleration term to the natural dynamics previously derived. In order to add additional thrust terms to the CR3BP, the equations of motions are written as

$$\dot{\vec{x}} = \vec{f} = \begin{bmatrix} \vec{v} \\ U_r^* + \vec{h}\left(\vec{v}\right) + \vec{a}_{thrust} \end{bmatrix} \tag{2.75}$$

Here, $\vec{u}$ is the control throttle vector defined such that $\hat{u}$ represents the thrust direction and $0 \leq |\vec{u}| \leq 1$ represents the control throttle magnitude. The throttle magnitude represents the extent to which the thrusters are firing. A value of 0 corresponds to the thrusters being inactive, while $|\vec{u}| = 1$ corresponds to the thrusters firing at max capacity. T represents the maximum non-dimensional thrust value and is a characteristic of the propulsive system used. The acceleration due to the thrust introduced by the spacecraft propulsion system is denoted by $\vec{a}_{thrust}$ and is defined as

$$\vec{a}_{thrust} = \frac{T}{m}\vec{u} \tag{2.76}$$

where m represents the non dimensional mass of the spacecraft and is defined as

$$m = \frac{\tilde{M}_3}{\tilde{m}_0} \tag{2.77}$$

where, $\tilde{M}_3$ is the spacecraft mass and $\tilde{m}_0$ is the initial dimensional spacecraft mass. The dimensional mass flow rate of the spacecraft can be written as[6]

$$\dot{\tilde{M}}_3 = -\frac{\tilde{T}_{max}|\vec{u}|}{\tilde{I}_{sp}\tilde{g}_0} \tag{2.78}$$

where, $\tilde{I}_{sp}$ represents the dimensional specific impulse of the propulsive system. The maximum dimensional thrust is denoted by $\tilde{T}_{max}$ and $\tilde{g}_0$ is the acceleration due to gravity on the earth.

Next, non dimensional maximum thrust and the non dimensional mass flow rate are defined as

$$T = \frac{\tilde{T}_{max}\left(t^*\right)^2}{l^*\tilde{m}_0} \tag{2.79}$$

$$\dot{m} = -c|\vec{u}| \tag{2.80}$$

$$c = \frac{\tilde{T}_{max} t^*}{\tilde{I}_{sp} \tilde{g}_0 \tilde{m}_0} \tag{2.81}$$

Finally, the equations of motion for a state vector $\vec{x} = \begin{bmatrix} \vec{r} \\ \vec{v} \\ m \end{bmatrix}$ are written as

$$\dot{\vec{x}} = \vec{f} = \begin{bmatrix} \vec{v} \\ U_r^* + \vec{h}\left(\vec{v}\right) + \frac{T}{m}\vec{u} \\ -c|\vec{u}| \end{bmatrix} \tag{2.82}$$

Chapter 3

Numerically Correcting Trajectories

Due to the nonlinear nature of the CR3BP, corrections procedures are utilized to generate a continuous trajectory from an initial guess. This process is carried out multiple times in order to achieve the desired conditions. In this work, a multiple shooting corrections procedure has been used to generate transfers.

3.1 Multiple shooting

The multiple shooting scheme is used to correct trajectories. In this method, a number of discontinuous arcs are set up as shown in Fig 3.1. Each arc is completely defined by a vector called the free variable vector. The expression is as follows

$$\vec{V}_i = \begin{bmatrix} \vec{x}_{i,0} \\ \Delta t_i \end{bmatrix} \tag{3.1}$$

Here, $\vec{x}_{i,0}$ represents the initial state vector for the i$^{\text{th}}$ arc and Δt_i represents the time of flight of the i$^{\text{th}}$ arc. The combined free variable vector is defined as follows

$$\vec{V} = \begin{bmatrix} \vec{V}_1 \\ \vec{V}_2 \\ \vec{V}_3 \\ \vdots \\ \vec{V}_n \end{bmatrix} \tag{3.2}$$

where n represents the number of arcs. A constraint vector $\vec{F}$ is defined to include all the constraint equations, where $\vec{F} = \vec{0}$ indicates that the constraints are satisfied. The goal of the corrections procedure is to update the free variable vector in order to drive the constraint vectors to as close to 0 as possible. Due to numerical precision issues, the procedure is said to have converged if the norm of the constraint vectors falls below some small tolerance value.

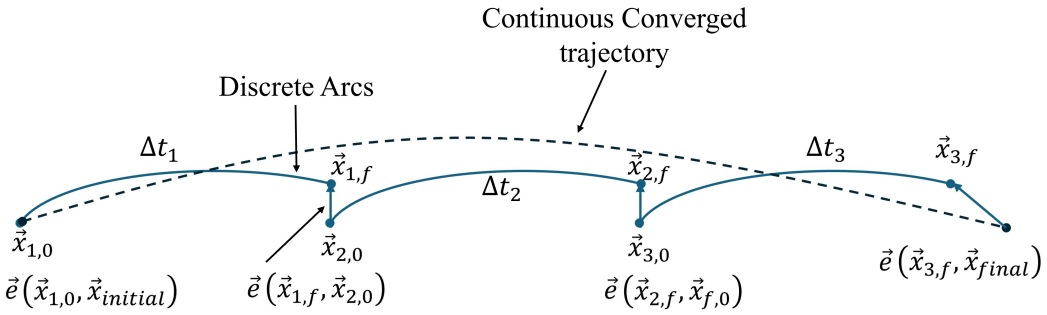

Figure 3.1: Multiple Shooting corrections procedure

Assuming there exists a desired solution $\vec{V}^*$ close to the initial guess $\vec{V}_0$ such that $\vec{F}\left(\vec{V}^*\right) = \vec{0}$ is satisfied, a first-order Taylor series expansion is used as follows

$$\vec{F}\left(\vec{V}^*\right) = \vec{0} = \vec{F}\left(\vec{V}_0\right) + \left.\frac{\partial \vec{F}}{\partial \vec{V}}\right|_{\vec{V}_0} \delta\vec{V} \tag{3.3}$$

Thus, the correction to the free variable vector $\delta\vec{V}$ can be obtained by inverting the Jacobian matrix $\left.\frac{\partial \vec{F}}{\partial \vec{V}}\right|_{\vec{V}_0}$. If the Jacobian matrix is not square, the minimum norm solution is used

$$\delta\vec{V} = \left[\frac{\partial \vec{F}}{\partial \vec{V}}\right]^\top \left[\left[\frac{\partial \vec{F}}{\partial \vec{V}}\right]\left[\frac{\partial \vec{F}}{\partial \vec{V}}\right]^\top\right]^{-1} \vec{F}\left(\vec{V}_0\right) \tag{3.4}$$

The free variable vector update equation is written as

$$\vec{V}^{i+1} = \vec{V}^i - J^\top \left[JJ^\top\right]^{-1} \vec{F}\left(\vec{V}^i\right) \tag{3.5}$$

where, J is the Jacobian matrix and is given by $J = \left.\left[\frac{\partial \vec{F}}{\partial \vec{V}}\right]\right|_{\vec{V}^i}$. The i superscript represents the i^{th} iteration. The constraint vectors for interior arcs (all arcs except the last arc) are defined

below

$$\vec{F}_i = \begin{bmatrix} \vec{x}_{i,f} - \vec{x}_{i+1,0} \end{bmatrix} \tag{3.6}$$

where, $\vec{x}_{initial}$ and $\vec{x}_{final}$ are specific state vectors the solution must begin and end at. Thus, the initial and final constraint vectors $\vec{F}_0$ and $\vec{F}_f$ are defined so as to ensure the trajectory starts and ends at a specific desired state. Constraint vectors can be modified based on the requirements of the trajectories to be generated.

$$\vec{F}_f = \begin{bmatrix} \vec{x}_{n,f} - \vec{x}_{final} \end{bmatrix} \tag{3.7}$$

$$\vec{F}_0 = \begin{bmatrix} \vec{x}_{1,0} - \vec{x}_{inital} \end{bmatrix} \tag{3.8}$$

All constraint equations are collected, similar to how the complete free variable vector was assembled. The Jacobian Matrix is formulated as

$$J = \frac{\partial \vec{F}}{\partial \vec{V}} = \begin{bmatrix} \frac{\partial \vec{F}_1}{\partial \vec{V}_1} & \frac{\partial \vec{F}_1}{\partial \vec{V}_2} & 0 & \cdots & \cdots \\ 0 & \frac{\partial \vec{F}_2}{\partial \vec{V}_2} & \frac{\partial \vec{F}_2}{\partial \vec{V}_3} & \ddots & \cdots \\ \vdots & \ddots & \ddots & \ddots & \ddots \\ \vdots & & 0 & \frac{\partial \vec{F}_{n-1}}{\partial \vec{V}_{n-1}} & \frac{\partial \vec{F}_{n-1}}{\partial \vec{V}_n} \\ \vdots & & & 0 & \frac{\partial \vec{F}_f}{\partial \vec{V}_n} \\ \frac{\partial \vec{F}_0}{\partial \vec{V}_1} & 0 & \cdots & \cdots & 0 \end{bmatrix} \tag{3.9}$$

The component blocks of the Jacobian Matrix are defined below

$$\frac{\partial \vec{F}_i}{\partial \vec{V}_i} = \begin{bmatrix} \phi_i & \dot{\vec{x}}_{i,f} \end{bmatrix}_{6\times 7} \tag{3.10}$$

$$\frac{\partial \vec{F}_i}{\partial \vec{V}_{i+1}} = \begin{bmatrix} -I_{6\times 6} & 0_{14\times 1} \end{bmatrix}_{6\times 7} \tag{3.11}$$

$$\frac{\partial \vec{F}_0}{\partial \vec{V}_1} = \begin{bmatrix} I_{6\times 6} & 0_{6\times 1} \end{bmatrix}_{6\times 7} \tag{3.12}$$

$$\frac{\partial \vec{F}_f}{\partial \vec{V}_n} = \begin{bmatrix} \phi_n & \dot{\vec{x}}_{n,f} \end{bmatrix}_{6\times 7} \tag{3.13}$$

3.2 Natural Parameter Continuation

Continuation is a powerful technique to leverage an existing, known solution, in order to generate a solution lying sufficiently close to it. Using the current known solution, and by modifying the constraints slightly, a new solution in the vicinity of the original can be found. This technique is extensively utilized in this thesis in order to transition from an initial guess low thrust trajectory to a final optimal transfer. This is done by slowly varying the constraints in order to enforce all conditions necessary for optimality, as defined in Chapter 4. However, a vital part of this procedure, is that the original solution must lie sufficiently close to the desired new solution. However, due to the chaotic nonlinear nature of the CR3BP, and differing sensitivities across regions of the solution space, there is no formal definition of what counts as 'sufficiently close'. Care must be taken to avoid attempting too large of a jump in parameters to be varied. This can result in ill conditioned Jacobian matrices and lead to suboptimal solutions due to lack of accuracy. The formulation of the free variables and constraint vectors remains the same as before. The difference here is that the constraint values are slowly changed in order to compute different solutions. Fig 3.2 depicts thisprocess, where s is some parameter to be varied.

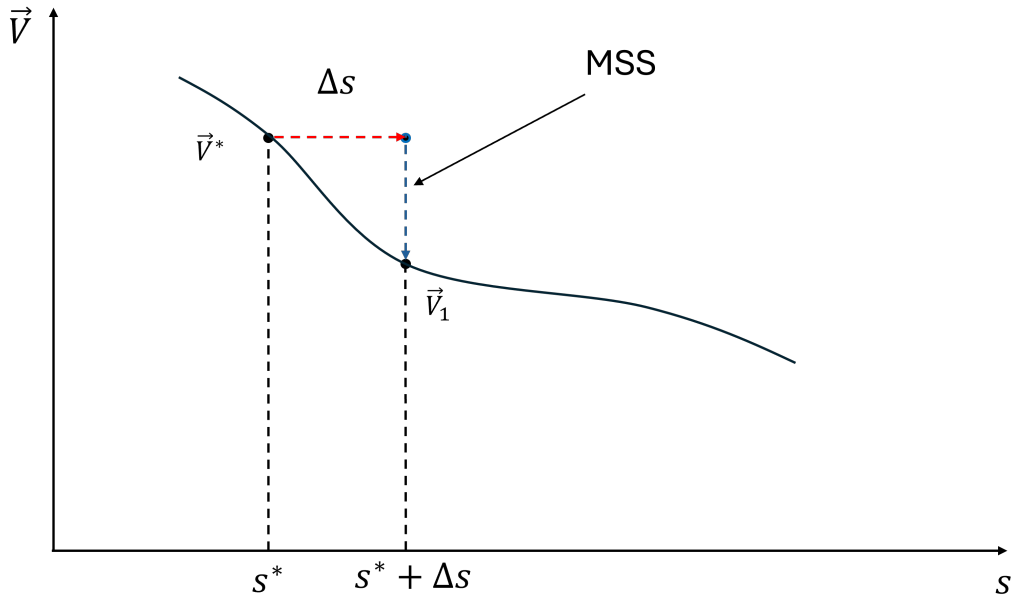

Figure 3.2: Natural parameter continuation

Chapter 4

Optimal Control

4.1 General Formulation

This section details the procedure involved in setting up an indirect optimization problem and deriving the necessary conditions to ensure optimality. Considering a state vector $\vec{x}$ and a control vector $\vec{u}$, the system dynamics are written as

$$\dot{\vec{x}} = \vec{f}\left(\vec{x}, \vec{u}, t\right) \tag{4.1}$$

The optimization problem has some constraints to be satisfied as a function of the initial and final states and times. Thus, the expression for the constraints are given as a vector Ψ and are written in a form, which when set to zero indicates that he constraints are satisfied.

$$\vec{\Psi}\left(\vec{x}_0, \vec{x}_f, t_0, t_f\right) = \vec{0} \tag{4.2}$$

Next, the goal of the optimization problem is defined by defining a scalar cost function J_{cost} which is to be minimized. The cost function can, in general, be written as a function of the initial and final states and time, as well as a Lagrangian function, which is itself a function of the state, control vector and time. Thus, the cost function is written as

$$J_{cost} = K\left(\vec{x}_0, \vec{x}_f, t_0, t_f\right) + \int_{t_0}^{t_f} L\left(\vec{x}, \vec{u}, t\right) dt \tag{4.3}$$

Next, the Hamiltonian is formulated as follows

$$H = \vec{p}(t) \cdot \vec{f}\left(\vec{x}, \vec{u}, t\right) + L\left(\vec{x}, \vec{u}, t\right) \tag{4.4}$$

$\vec{p}(t)$ is a newly introduced vector called the costate vector. They are functions of time. While they have no physical meaning, they help in finding optimal solutions by satisfying the necessary conditions derived later[3, 7]

In order to minimize the defined cost function, the associated Hamiltonian must be minimized. A fundamental concept involved in optimal control theory is Pontryagin's minimum principle. This states that for a defined cost function, there exists a particular control vector time history $\vec{u}^*$, such that the defined cost function is minimized. Any deviation from this particular control vector time history results in a non optimal solution. The goal of optimization is to determine this particular control and substitute it back into the expression for the Hamiltonian. Thus, the minimized Hamiltonian is written as

$$H^*\left(\vec{x},\vec{p},t\right)=\vec{p}\left(t\right).\vec{f}\left(\vec{x},\vec{u}^*\left(\vec{x},\vec{p},t\right),t\right)+L\left(\vec{x},\vec{u}^*\left(\vec{x},\vec{p},t\right),t\right) \tag{4.5}$$

The system and costate dynamics are then given by

$$\dot{\vec{x}}\left(t\right)=\left[\frac{\partial H^*}{\partial\vec{p}}\right]^T \tag{4.6}$$

$$\dot{\vec{p}}(t)=-\left[\frac{\partial H^*}{\partial\vec{x}}\right]^T \tag{4.7}$$

Necessary conditions regarding the initial and final costates and Hamiltonian are determined using the transversality conditions, and are dependent on the form of the cost function and the constraint vector $\vec{\Psi}$

$$\vec{p_0}=-\frac{\partial K}{\partial\vec{x}_0}-\vec{\lambda}\cdot\frac{\partial\vec{\Psi}}{\partial\vec{x}_0} \tag{4.8}$$

$$\vec{p_f}=\frac{\partial K}{\partial\vec{x}_f}+\vec{\lambda}\cdot\frac{\partial\vec{\Psi}}{\partial\vec{x}_f} \tag{4.9}$$

$$H_0=\frac{\partial K}{\partial t_0}+\vec{\lambda}\cdot\frac{\partial\vec{\Psi}}{\partial t_0} \tag{4.10}$$

$$H_f=-\frac{\partial K}{\partial t_f}-\vec{\lambda}\cdot\frac{\partial\vec{\Psi}}{\partial t_f} \tag{4.11}$$

In order for a solution to be optimal, there must exist costates which satisfy the costate dynamics as well as the above defined transversality conditions.

4.2 Primer Vector Theory Formulation

Primer vector theory is a form of indirect optimal control as applied to the optimization of spacecraft trajectories. The system is defined using a state vector as follows

$$\vec{x} = \begin{bmatrix} \vec{r}^{\,T} & \vec{v}^{\,T} & m \end{bmatrix}^T \tag{4.12}$$

Where, $\vec{r}$, $\vec{v}$ and m denote the spacecraft position vector, velocity vector and non dimensional mass of the spacecraft.

The system dynamics defined in Chapter 2 are used

$$\dot{\vec{x}} = \vec{f} = \begin{bmatrix} \vec{v} \\ \frac{\partial U^*}{\partial \vec{r}} + \vec{h} + \frac{T}{m}|\vec{u}|\hat{u} \\ -c|\vec{u}| \end{bmatrix} \tag{4.13}$$

The constraint vector for the current optimization problem is set up as follows

$$\vec{\Psi} = \begin{bmatrix} |\vec{e}_0| - e_{des} \\ |\vec{r}_0| - |r_{des}| \\ m_0 - 1 \\ \vec{r}_f - \vec{r}_{target} \\ \vec{v}_f - \vec{v}_{target} \end{bmatrix} \tag{4.14}$$

where, $|\vec{r}_0|$ and $|\vec{e}_0|$ denote the initial distance of the spacecraft from Saturn, and the initial eccentricity of the spacecraft with respect to Saturn in the two body problem. The constraints ensure that these are fixed at specific values. It is desired that hard constraints be enforced on the final position and state vectors, in order to ensure that the spacecraft inserts onto a particular state along the target orbit. The constraint on the spacecraft mass at t_0 ensures that the solution begins with 100% of the spacecraft mass available. Next, the cost function to be minimized is set up as follows

$$J_{cost} = \int_{t_0}^{t_f} c|\vec{u}|dt \tag{4.15}$$

This cost function definition aims to minimize the mass flow rate of the spacecraft. This is analogous to defining a cost function to maximize the final spacecraft mass. Using the defined cost function, the Hamiltonian is defined as follows

$$H\left(\vec{x},\vec{u},\vec{p},t\right)=\vec{p}_r\cdot\vec{v}+\vec{p}_v\cdot\left(\frac{\partial U^*}{\partial\vec{r}}+\vec{h}\left(\vec{v}\right)+\frac{T}{m}|\vec{u}|\hat{u}\right)-p_m c|\vec{u}|+c|\vec{u}| \tag{4.16}$$

In order to minimize the Hamiltonian, we can observe individual terms involving the control vector. The only term involving the control vector direction is the dot product between the velocity costate vector and the control vector. Minimizing this term is necessary for the Hamiltonian to be minimized. Thus we obtain an expression for the control vector direction

$$\hat{u}^*=-\frac{\vec{p}_v}{|\vec{p}_v|} \tag{4.17}$$

Substituting the expression for the control vector direction back into Equation 4.16, the Hamiltonian can be rewritten as

$$H\left(\vec{x},\vec{u},\vec{p},t\right)=\vec{p}_r\cdot\vec{v}+\vec{p}_v\cdot\left(\frac{\partial U^*}{\partial\vec{r}}+\vec{h}\left(\vec{v}\right)\right)+Sc|\vec{u}| \tag{4.18}$$

where, S is a switching function and is defined as

$$S=\left(1-p_m-\frac{T|\vec{p}_v|}{mc}\right) \tag{4.19}$$

We observe that the control throttle magnitude $|\vec{u}|$ depends on the sign of the switching function. Thus,

$$|\vec{u}^*|=\begin{cases}1 & S<0\\ \\ 0 & S>0\end{cases} \tag{4.20}$$

Thus, the optimal control throttle magnitude must follow a bang-bang profile, depending on the switching parameter. The costate dynamics are derived as follows

$$\dot{\vec{p}}_r=-\left(\frac{\partial H}{\partial\vec{r}}\right)^T=-\frac{\partial}{\partial\vec{r}}\left(\vec{p}_r\cdot\frac{\partial U*}{\partial\vec{r}}\right)^T=-\left[\frac{\partial^2 U^*}{\partial\vec{r}^{\,2}}\right]^T\vec{p}_r \tag{4.21}$$

$$\dot{\vec{p}}_v=-\left(\frac{\partial H}{\partial\vec{v}}\right)^T=-\frac{\partial}{\partial\vec{v}}\left(\vec{p}_r\cdot\vec{v}+\vec{p}_v\cdot\vec{h}\left(\vec{v}\right)\right)^T=-\vec{p}_r-\left[\frac{\partial\vec{h}\left(\vec{v}\right)}{\partial\vec{v}}\right]^T\vec{p}_v \tag{4.22}$$

$$\dot{p}_m = -\frac{\partial H}{\partial m} = -\frac{T|\vec{p}_v|}{m^2}|\vec{u}| \tag{4.23}$$

Utilizing these defined constraints, the transversality conditions are determined.

$$p_m\left(t_f\right) = 0 \tag{4.24}$$

$$H_0 = 0 \tag{4.25}$$

$$H_f = 0 \tag{4.26}$$

Although the formulated optimization problem uses an unconstrained time of flight formulation, it is important to note that the final optimal solution will have a time of flight close to that of the initial guess trajectory used. If time of flight is to be constrained, the relevant constraints are added to $\vec{\Phi}$ and the constraints on the initial and final Hamiltonian are removed.

4.3 Smoothing

It has been shown in the previous section that the optimal control throttle magnitude must follow a bang-bang profile. However, incorporating bang-bang control profiles introduce certain issues. Due to the rapid switching of the control throttle magnitude, the discontinuities introduces large sensitivities in the numerical solver used. In order to avoid this, the optimal control throttle magnitude is rewritten as a hyperbolic function, utilizing a parameter ϵ [21, 22]

$$|\vec{u}^*| = \frac{1}{2}\left(1 - \tanh\left(\frac{S}{\epsilon}\right)\right) \tag{4.27}$$

As $\epsilon \to 0$, the smoothed control throttle magnitude will approach the required bang-bang profile. This is demonstrated in Figure 4.1. The initial value of ϵ is set to 1. Once all other necessary conditions and constraints are satisfied, natural parameter continuations is used to transition ϵ to a near zero value. The hyperbolic smoothing approach has been shown to be more effective over the traditional homotopy smoothing [18].

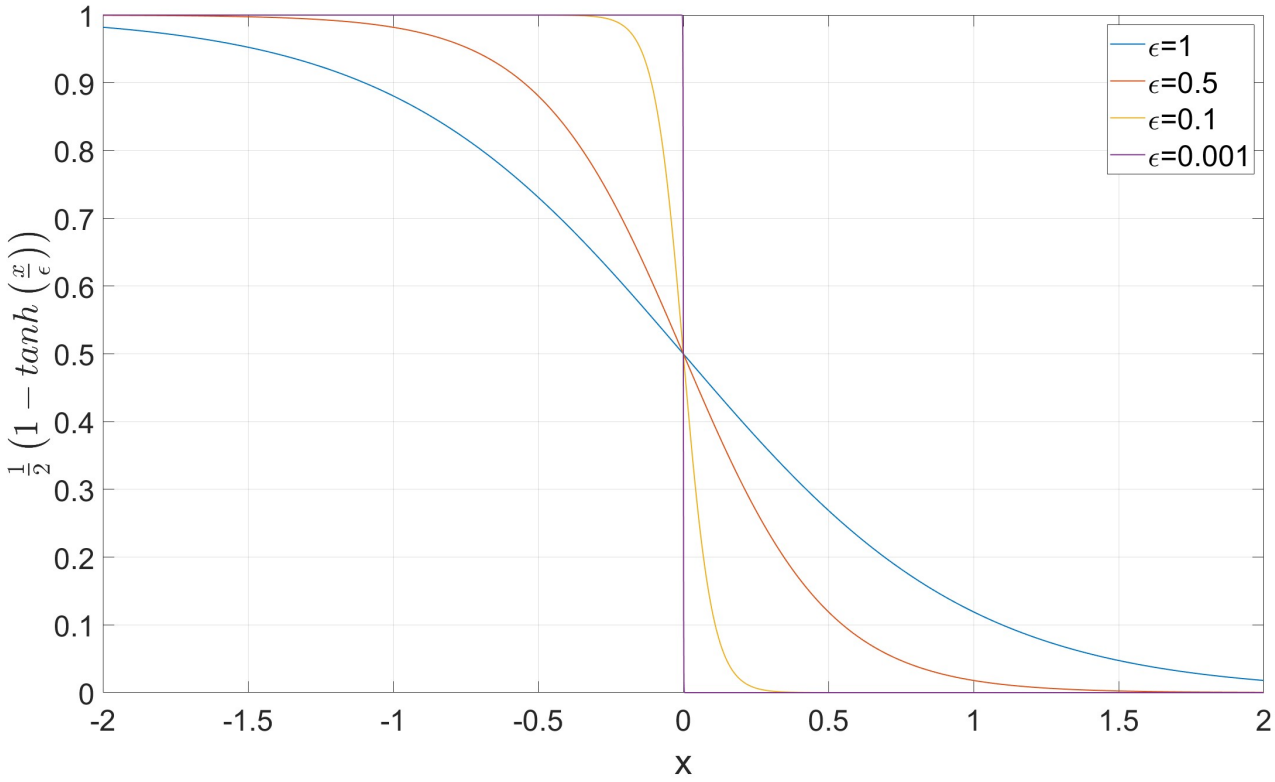

Figure 4.1: Smoothened control throttle magnitude

4.4 Modified State Transition Matrix

A new state vector is defined, incorporating the spacecraft position, velocity, mass as well as their associated costates

$$\vec{y} = \begin{bmatrix} \vec{r}^{\,T} & \vec{v}^{\,T} & m & \vec{p}_r{}^{\,T} & \vec{p}_v{}^{\,T} & p_m \end{bmatrix}^T \tag{4.28}$$

The new state transition matrix is still denoted by ϕ. $[A]$ is given by

$$[A] = \begin{bmatrix} 0_{3\times3} & I_{3\times3} & 0_{3\times1} & 0_{3\times3} & 0_{3\times3} & 0_{3\times1} \\ U^*_{rr} & \vec{h}_v & A_1 & 0_{3\times3} & A_2 & A_3 \\ 0_{1\times3} & 0_{1\times3} & A_4 & 0_{1\times3} & A_5 & A_6 \\ A_7 & 0_{3\times3} & 0_{3\times1} & 0_{3\times3} & -\left(U^*_{rr}\right)^T & 0_{3\times1} \\ 0_{3\times3} & 0_{3\times3} & 0_{3\times1} & -I_{3\times3} & -\left[\frac{\partial\vec{h}(\vec{v})}{\partial\vec{v}}\right]^T & 0_{3\times1} \\ 0_{1\times3} & 0_{1\times3} & A_8 & 0_{1\times3} & A_9 & A_{10} \end{bmatrix} \tag{4.29}$$

Where,

$$A_1 = -\frac{T\vec{p}_v}{m|\vec{p}_v|}\frac{\partial|u|}{\partial m} - \frac{T\vec{u}^*}{m^2} \tag{4.30}$$

$$A_2 = \frac{T}{m}\frac{\partial\vec{u}}{\partial\vec{p}_v} \tag{4.31}$$

$$A_3 = \frac{-T\vec{p}_v}{m|\vec{p}_v|}\frac{\partial|\vec{u}|}{\partial p_m} \tag{4.32}$$

$$A_4 = -b\frac{\partial|\vec{u}|}{\partial m} \tag{4.33}$$

$$A_5 = -b\frac{\partial|\vec{u}|}{\partial\vec{p}_v} \tag{4.34}$$

$$A_6 = -b\frac{\partial|\vec{u}|}{\partial p_m} \tag{4.35}$$

$$A_7 = -\frac{\partial\left(U^*_{rr}\vec{p}_v\right)}{\partial\vec{r}} \tag{4.36}$$

$$A_8 = -\frac{T|\vec{p}_m|}{m^2}\frac{\partial|\vec{u}|}{\partial m} + \frac{2T|\vec{p}_v||\vec{u}|}{m^3} \tag{4.37}$$

$$A_9 = -\frac{T|\vec{p}_m|}{m^2}\frac{\partial|\vec{u}|}{\partial\vec{p}_v} - \frac{T|\vec{u}|\vec{p}_v^{\top}}{|\vec{p}_v|m^2} \tag{4.38}$$

$$A_{10} = -\frac{T|\vec{p}_v|}{m^2}\frac{\partial|\vec{u}|}{\partial p_m} \tag{4.39}$$

The derivatives of the control vector and its magnitude are found to be

$$\frac{\partial|\vec{u}|}{\partial m} = -\frac{T|\vec{p}_v|}{2\epsilon bm^2}\left(1 - tanh^2\left(\frac{S}{\epsilon}\right)\right) \tag{4.40}$$

$$\frac{\partial|\vec{u}|}{\partial p_m} = \frac{1}{2\epsilon}\left(1 - tanh^2\left(\frac{S}{\epsilon}\right)\right) \tag{4.41}$$

$$\frac{\partial|\vec{u}|}{\partial\vec{p}_v} = \frac{T}{2\epsilon bm|\vec{p}_v|}\left(1 - tanh^2\left(\frac{S}{\epsilon}\right)\right)\vec{p}_v^{\top} \tag{4.42}$$

$$\frac{\partial\vec{u}}{\partial\vec{p}_v} = -\frac{T}{2\epsilon bm|\vec{p}_v|^2}\left(1 - tanh^2\left(\frac{S}{\epsilon}\right)\right)\vec{p}_v\vec{p}_v^{\top} - \left(I_{3\times3} - \frac{\vec{p}_v\vec{p}_v^{\top}}{|\vec{p}_v|^2}\right)\frac{|\vec{u}|}{|\vec{p}_v|} \tag{4.43}$$

Chapter 5

Technical Approach

One of the most important aspects of solving an optimization problem by means of an indirect approach, is the generation of an initial guess trajectory. Any solution to be obtained must lie reasonably close to the initial guess. The definition of varies based on several factors, such as the problem formulation and dynamical model used. In the current formulation, this is extremely important due to the chaotic and nonlinear nature of the CR3BP. This chapter describes the method used to generate the initial guess. Once a suitable guess is constructed, the approach used to converge to the final propellant mass optimal solution is defined. In addition, this chapter also describes the system parameters and propulsive system properties utilized.

5.1 Spacecraft Parameters

The characteristic quantities required to characterize the Saturn-Titan CR3BP dynamical model as defined in Chapter 2, are as follows

l^* (km)	t^* (s)	$\tilde{M}_1(kg)$	$\tilde{M}_2(kg)$	μ
1221900	219282.401464932	5.68336103×10^{26}	1.3452246×10^{23}	0.000236639258605855

Table 5.1: Characteristic quantities of the Saturn-Titan CR3BP dynamical model

Next, the propulsive system is chosen to be modeled after an SPT-140 Hall effect thruster [19] which is currently being used aboard the Psyche 1 mission. 3 of these thrusters are chosen to be used for the defined problem. These quantities, as well as the spacecraft mass are defined in Table 5.2. Using the notation defined in Chapter 2, dimensional quantities are denoted by a ˜

$\tilde{T}_{max}$ (N)	$\tilde{I}_{sp}$ (s)	$\tilde{M}_3$ (kg)
0.84	1800	3000

Table 5.2: Spacecraft Propulsive System specifications

5.2 Target Orbits and States

The target orbits are chosen to be an L_1 northern Halo orbit and an L_2 Vertical Orbit, due to the close passes to the polar regions of Titan and the fact that both orbits allow for views of the polar regions for a large part of the orbital period. The target Halo orbit is shown in Fig 5.1

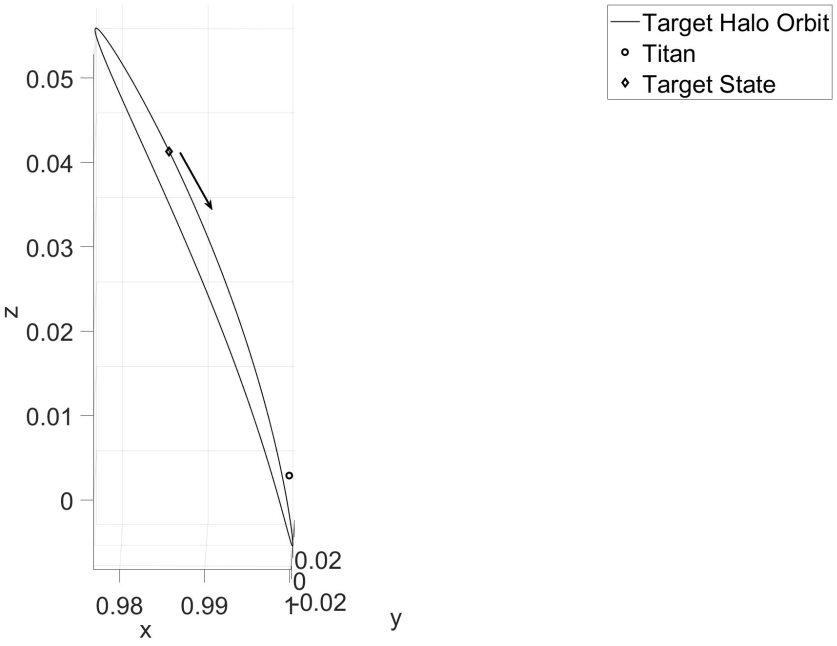

Figure 5.1: Target L_1 Halo orbit

The selection of a particular state along the orbit is an extremely important part of the solution process. It is desired to target a state lying sufficiently far enough away from the primary so as to not introduce highly sensitive trajectories, which would cause issues with the corrections procedure. In addition, as the trajectory will approach from the left with respect to the x direction, a target state with a positive velocity in the x direction is chosen in order to avoid complex directional changes which would lead to an extremely sensitive corrections procedure. Similarly,

the target Vertical orbit and the target state along it are shown in Fig 5.2

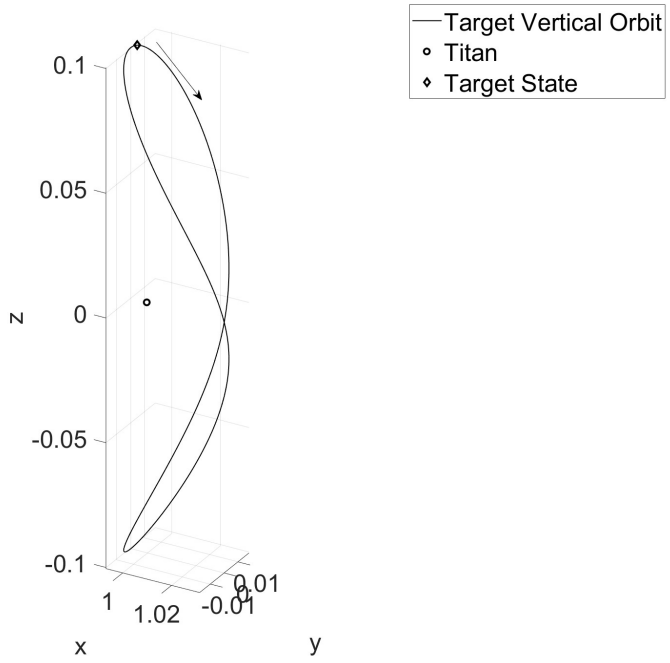

Figure 5.2: Target L_2 Vertical orbit

The specific target states and orbit characteristics are as follows

	Halo orbit	Vertical orbit
x	0.953877547560189	0.993603919932203
y	0.0369323860081236	0.00409866676552211
z	0.201221128938578	0.0996943569336411
$\dot{x}$	0.0680049340806129	0.00789914331709248
$\dot{y}$	0.0279908952266641	0.0365268937582515
$\dot{z}$	-0.25576126140558	-0.0136829056017508
Jacobi Constant	3.00327905281339	2.99227140457312
Orbit period (Days)	5.04273266085836	13.2483117551729

Table 5.3: Characteristics of target states on each orbit

5.3 Boundary Conditions

The boundary conditions are chosen so as to ensure the spacecraft begins at a distance of 400000 km away from the center of Saturn, with an eccentricity in the two body problem of 0.3.

These values were chosen to resemble past interplanetary missions, which arrive at gas giants such as Jupiter and Saturn, with an eccentric orbit. However, previous missions arrived at much larger eccentricities. These values can be varied as desired. Hard constraints are placed on the spacecraft final position and velocity states in order to ensure insertion onto the desired orbits.

5.4 Initial Guess Construction

Due to the incorporation of low thrust propulsion as opposed to impulsive maneuvers, initial trajectories incorporating spiral out motions to escape the vicinity of Saturn have been utilized in order to slowly change the Jacobi constant.

In order to generate an initial trajectory guess, it is decided to choose the position and velocity costates at t_0 so as to ensure that the spacecraft is thrusting purely along the initial velocity vector at t_0. This choice was made to keep the initial trajectory design procedure simple. Thus, we have

$$\hat{u}^* = \frac{\vec{v}_0}{|\vec{v}_0|} = -\frac{\vec{p}_{v_0}}{|\vec{p}_{v_0}|} \tag{5.1}$$

$$\vec{p}_{v_0} = -\gamma \vec{v}_0 \tag{5.2}$$

γ is a small positive scalar value. The specific guidelines to choose the value of γ are explained in the following section. Utilizing Equation 4.22, an expression to determine the initial velocity costate is determined as follows

$$\vec{p}_{r_0} = \gamma \dot{\vec{v}} - \left[\frac{\partial \vec{h}\,(\vec{v})}{\partial \vec{v}}\right]^\top \vec{p}_{v_0} \tag{5.3}$$

Thus, for a fixed initial position and velocity state, γ and the initial mass costate p_m are the only parameters to be tuned. Finally, the time of flight is chosen upon successful selection of γ and p_m. The time of flight is chosen so as to ensure the trajectory closely approaches Titan without any complicated geometries in the obtained trajectory. The initial state is assumed to be a point corresponding to a planar circular orbit of radius 400000 km in the two body problem, lying on the X axis in the XY plane. The state has been chosen to attempt to mitigate the chaotic nature of trajectories in the CR3BP. The restriction of the trajectory to the XY plane avoids the chaotic nature of spatial orbits. Utilizing an initial state corresponding to an eccentric orbit results in

complicated trajectory geometries and loops. Using a circular state to begin with, allows us to more easily fine tune the parameters.

5.5 Guidelines to Choose Tuning Parameters

Although the described approach to generating the initial trajectory guess is essentially, trial and error, certain trends are noticed which can help guide the selection of the tuning parameters

5.5.1 Impact of p_m Value Selection

The effect of the initial mass costate on the trajectory design procedure is observed in Fig 5.3. The blue trajectory, corresponding to a larger value of the mass costate, deflects away from the vicinity of the primary, and departs the desired region. Reducing the mass costate allows the trajectory to remain bounded in the desired region. However, it is important to note that the flight time for the two trajectories is not the same. Thus, it is beneficial to utilize a large time of flight, while tuning the other parameters, and upon determining a trajectory which approaches the vicinity of Titan without complicated directional changes and other geometries, reduce the time of flight to achieve the first approach to Titan.

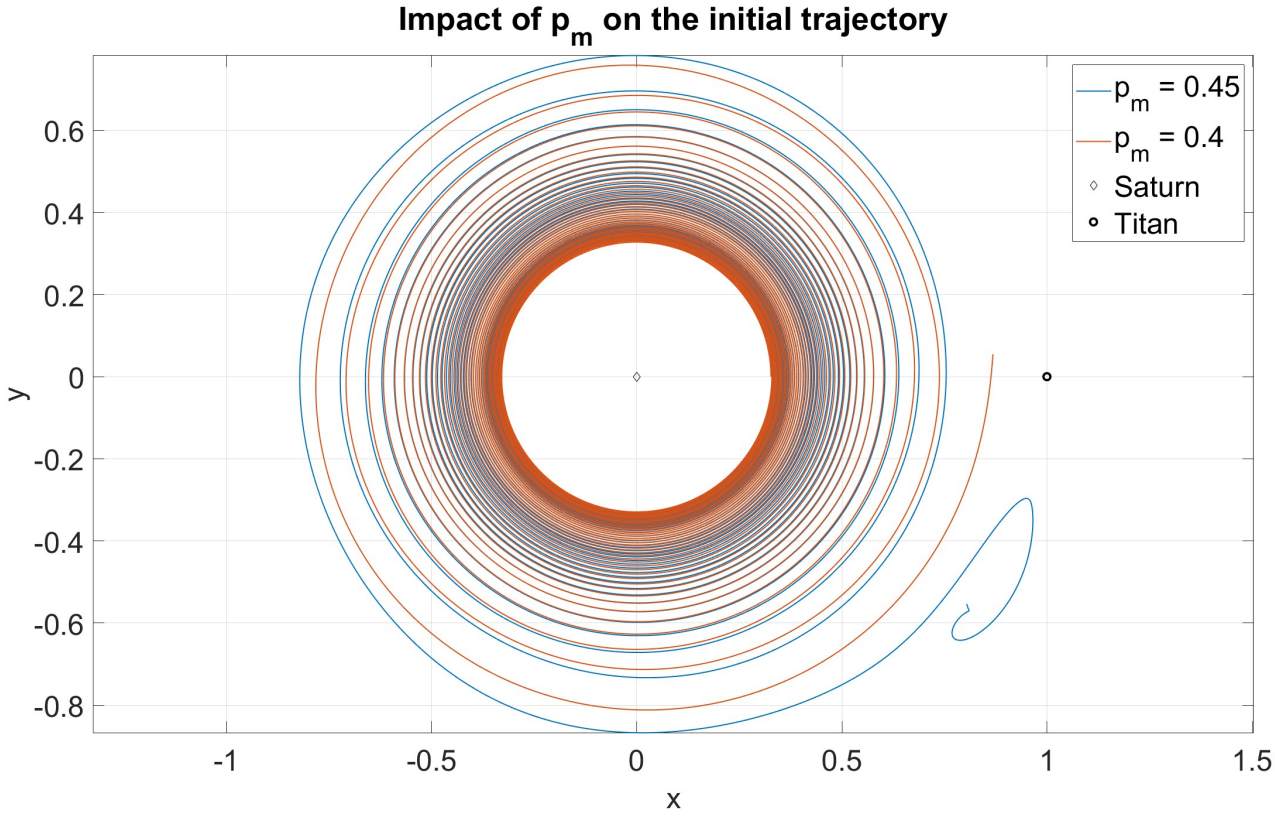

Figure 5.3: Impact of initial mass costate on trajectory guess

5.5.2 Impact of γ Value Selection

The effect of the choice of γ has a more complex effect on the trajectory design procedure. As seen from Fig 5.4, while the choice of γ clearly has an impact on the geometry of the generated trajectory, the tuning p_m can help to shape the trajectory as needed. A more useful diagnostic tool is the time evolution of the control throttle magnitude as seen in Fig 5.5. A larger value of γ results in a higher average control throttle magnitude. Raising the value of γ too high can result in a trajectory where the control throttle magnitude is near unity over the complete trajectory. It is observed that choosing γ corresponding to large average control throttle magnitudes adversely impacts the convergence to a propellant mass optimal solution. In addition, from a practical point of view, it is not desired to have a trajectory where the thrusters are firing at maximum capabilities for the entire flight time. The final propellant mass optimal solution control throttle magnitude

evolution is dependent on that of the initial trajectory. An initial trajectory with thrusters firing at near maximum capability will ensure a final solution where the control throttle magnitude is set to unity for close to the entire time of flight. Although this does technically satisfy the required bang-bang control profile, it is not desired to have thrusters firing over the entire trajectory.

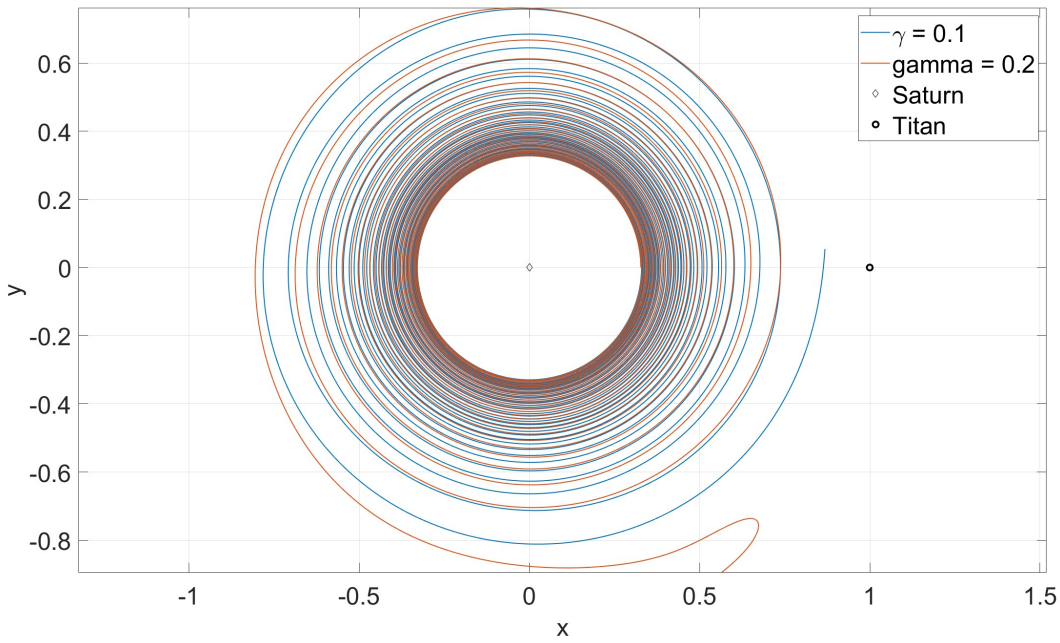

Figure 5.4: Impact of γ on the trajectory geometry

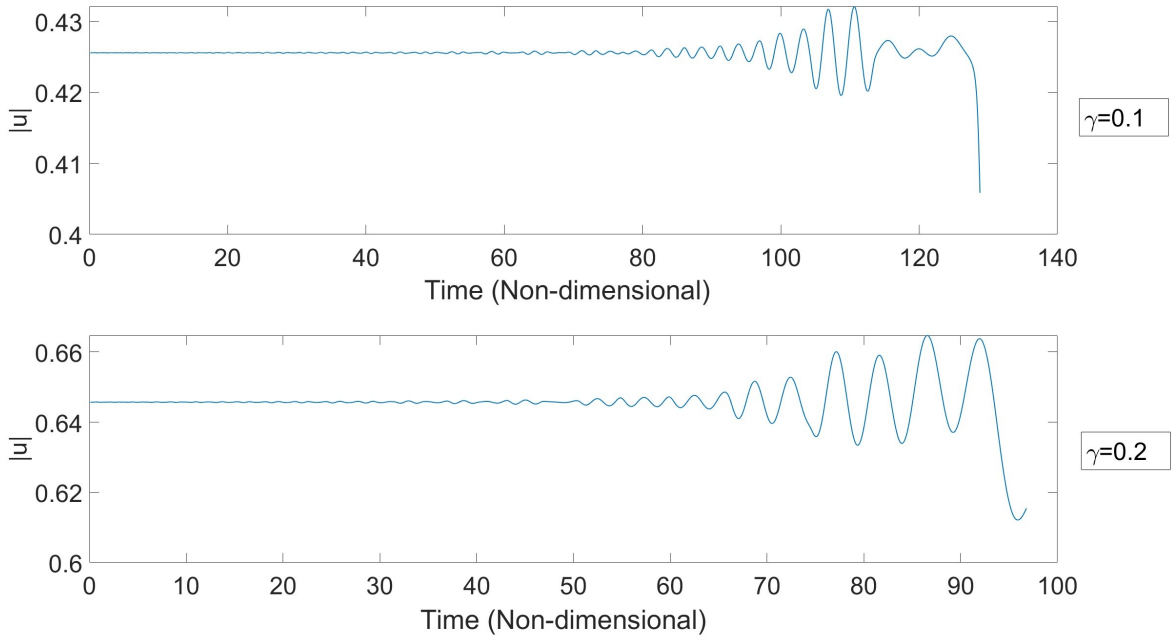

Figure 5.5: Impact of γ on the control throttle magnitude evolution

5.6 Transitioning to Spatial Trajectories

The approach defined to generate an initial trajectory results in purely planar trajectories. It is desired to obtain transfers resulting in insertions onto spatial orbits as defined in Chapter 2. In order to achieve thus, multiple shooting scheme and natural parameter continuation are utilized. The parameters to be varied are the constraints on the states, as well as the final mass costate, in order to satisfy the transversality conditions. It is important to ensure that the parameters are varied slowly, in small increments in order to ensure that the previous solution can be used as an initial guess with further change of parameters. In this step, ϵ is not varied. Once all other necessary constraints have been satisfied, natural parameter continuation is used to achieve $\epsilon \to 0$, in order to achieve a bang-bang control profile and thus, a propellant mass optimal solution.

5.7 Multiple Shooting Free Variables and Constraints

The augmented state vector defined in Chapter 4 is used to define the Free variable vector as

$$\vec{V}_i = \begin{bmatrix} \vec{y}_{i,0} \\ \Delta t_i \\ \beta_i \end{bmatrix} \tag{5.4}$$

where, Δt_i describes the time of flight of the i$^{\text{th}}$ arc, and β is a slack variable introduced to ensure each arc maintains a positive time of flight, as defined in the constraint vectors. The expression for the constraint vector for the interior arcs (all arcs except for the first and last) is defined as

$$\vec{F}_i = \begin{bmatrix} \vec{y}_{i,f} - \vec{y}_{i+1,0} \\ \Delta t_i - \beta_i^2 \end{bmatrix} \tag{5.5}$$

The required terminal constraints to be enforced are

- Non-dimensional mass at t_0 must be unity
- The state at t_0 must remain at a fixed distance from Saturn.
- The eccentricity at t_0 must be constrained
- The final position and velocity must equal the target state on the desired orbit.
- The final mass costate at t_f must be 0
- The initial and final Hamiltonian must be 0

Thus, the corresponding initial and final constraint vectors are formulated as follows

$$\vec{F}_f = \begin{bmatrix} \vec{x}_{n,f} - \vec{x}_d \\ \Delta t_n - \beta_n^2 \\ p_{m_{n,f}} \\ H_{n,f} \end{bmatrix} \tag{5.6}$$

$$\vec{F}_0 = \begin{bmatrix} |\vec{r}_{1,0}| - |r_{initial}| \\ |\vec{e}_{1,0}| - |e_{initial}| \\ m_{1,0} - 1 \\ H_{1,0} \end{bmatrix} \tag{5.7}$$

Thus, the Jacobian Matrix is formulated as follows

$$J = \frac{\partial \vec{F}}{\partial \vec{V}} = \begin{bmatrix} \frac{\partial \vec{F}_1}{\partial \vec{V}_1} & \frac{\partial \vec{F}_1}{\partial \vec{V}_2} & 0 & \cdots & \cdots \\ 0 & \frac{\partial \vec{F}_2}{\partial \vec{V}_2} & \frac{\partial \vec{F}_2}{\partial \vec{V}_3} & \ddots & \cdots \\ \vdots & \ddots & \ddots & \ddots & \ddots \\ \vdots & & 0 & \frac{\partial \vec{F}_{n-1}}{\partial \vec{V}_{n-1}} & \frac{\partial \vec{F}_{n-1}}{\partial \vec{V}_n} \\ \vdots & & & 0 & \frac{\partial \vec{F}_f}{\partial \vec{V}_n} \\ \frac{\partial \vec{F}_0}{\partial \vec{V}_1} & 0 & \cdots & \cdots & 0 \end{bmatrix} \tag{5.8}$$

The component blocks of the Jacobian Matrix are defined below

$$\frac{\partial \vec{F}_i}{\partial \vec{V}_i} = \begin{bmatrix} \phi_i & \dot{\vec{y}}_{i,f} & 0_{14\times 1} \\ 0_{1\times 14} & 1 & -2\beta_i \end{bmatrix}_{15\times 16} \tag{5.9}$$

$$\frac{\partial \vec{F}_i}{\partial \vec{V}_{i_1}} = \begin{bmatrix} -I_{14\times 14} & 0_{14\times 1} & 0_{14\times 1} \\ 0_{1\times 14} & 0 & 0 \end{bmatrix}_{15\times 16} \tag{5.10}$$

$$\frac{\partial \vec{F}_0}{\partial \vec{V}_1} = \begin{bmatrix} \frac{\partial |\vec{r}|}{\partial \vec{y}}\Big|_{1,0} & 0 & 0 \\ \frac{\partial |\vec{e}|}{\partial \vec{y}}\Big|_{1,0} & 0 & 0 \\ \phi_i\,(7, 1:14) & 0 & 0 \\ \frac{\partial H}{\partial \vec{y}}\Big|_{1,0} & 0 & 0 \end{bmatrix}_{4\times 16} \tag{5.11}$$

$$\frac{\partial \vec{F}_f}{\partial \vec{V}_n} = \begin{bmatrix} \phi_n\,(1:6, 1:14) & \dot{\vec{x}}_{n,f} & 0 \\ 0_{1\times 14} & 1 & -2\beta_n \\ \phi_n\,(14, 1:14) & \dot{p}_{m_{n,f}} & 0 \\ \frac{\partial H}{\partial \vec{y}}\Big|_{n,f} & 0 & 0 \end{bmatrix}_{9\times 16} \tag{5.12}$$

Chapter 6

Results

6.1 Transfer to an L_1 Halo Orbit

The procedure used to generate the initial guess described in Chapter 5 is utilized to generate an initial planar trajectory guess. Next, natural parameter continuation is used to transition to a spatial trajectory. As seen in Fig 6.1, the continuation procedure results in a transfer to the chosen state on the halo orbit. Although all necessary constraints have been enforced, the transfer is not propellant mass optimal, due to the lack of bang-bang control profile, as seen in the evolution of the control throttle magnitude over the transfer.

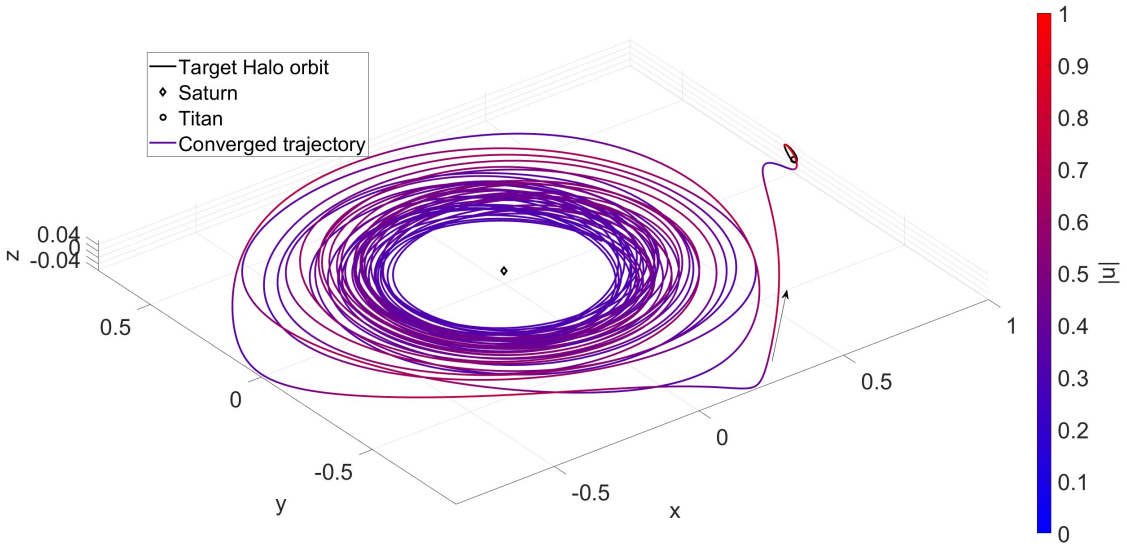

Figure 6.1: Converged result from continuation process for a transfer to an L_1 halo orbit

The transfer is characterized by a sharp directional change at approximately x = 0.2 and y = -0.8. Due to the nature of the continuation procedure, all subsequent solutions will retain this directional change structure. However, the specific position and extent may vary across solutions. The final step is to apply natural parameter continuation to reduce ϵ to arbitrarily close to 0 in order to achieve the required bang-bang control profile. The result after this step, is shown in Fig 6.2. As seen, the transfer cycles between periods of thrust and coast, corresponding to a bang-bang control profile. The transfer ends with a brief coast arc, followed by a final thrust arc to ensure orbit insertion.

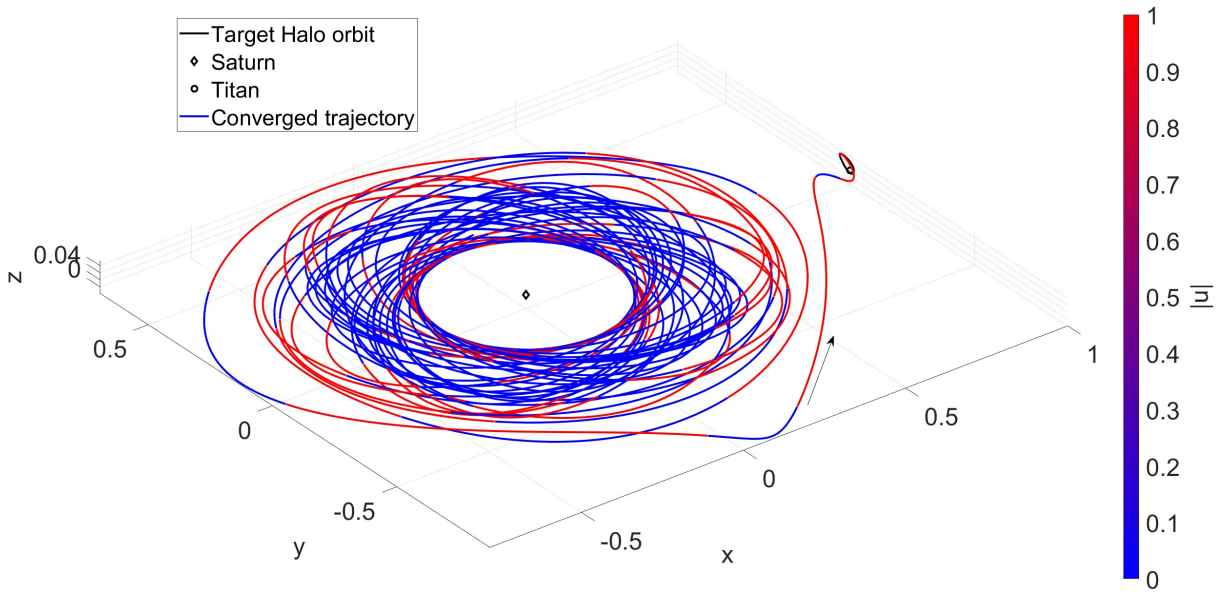

Figure 6.2: Converged result from continuation process for a propellant mass optimal transfer to an L_1 halo orbit in the CR3BP rotating frame

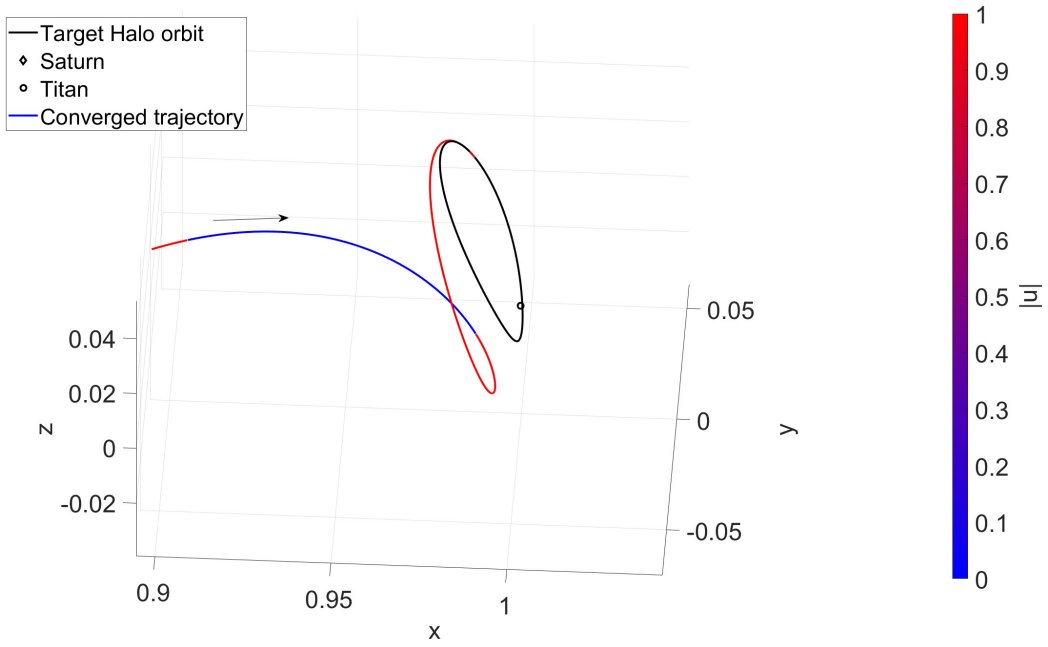

Figure 6.3: Zoomed in view of propellant mass optimal transfer to an L_1 halo orbit in the CR3BP rotating frame

The impact of the variation of ϵ can be studied through the change in propellant mass requirements as seen in Fig 6.4 and Table 6.1. As seen, there is a drastic improvement in the propellant requirements when comparing the smoothed control solution with the optimal bang-bang control profile solution, with a propellant requirement reduction of 122.13613839681 kg. A propellant requirement of 637.795 kg corresponds to approximately 21.26% of the total spacecraft mass. The propellant mass optimal propellant requirement of 515.6591 kg corresponds to 17.18% of the total mass. There is an improvement of approximately 4% of propellant mass usage, with respect to the total spacecraft mass. However, these values could vary, depending on the time of flight utilized. The difference in propellant mass requirements between a smoothed and a propellant mass optimal case may be more drastic when considering trajectories with shorter flight times.

ϵ	Propellant Usage (kg)
1	637.795221648746
0.9	628.95641705164
0.7	608.874799977247
0.5	583.901769132091
0.3	564.882959791697
0.1	543.354649962355
0.01	515.866035569523
0.0001	515.659083251936

Table 6.1: Impact of ϵ on propellant usage for transfer to an L_1 halo orbit

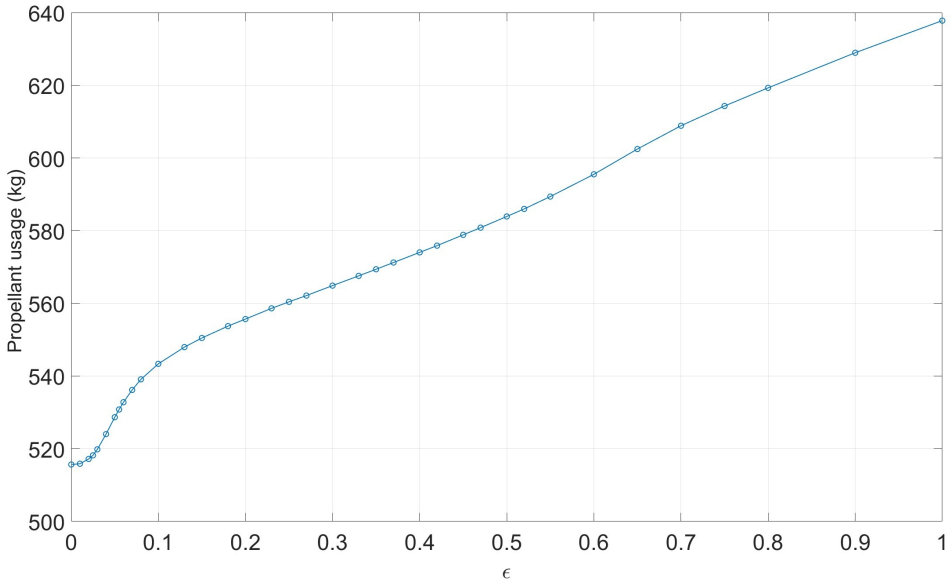

Figure 6.4: Effect of ϵ on propellant usage for transfer to an L_1 halo orbit

Next, Fig 6.5 proves that reducing ϵ results in bang-bang control profiles. In addition, the relationship between the control throttle magnitude and the switching parameter S is verified. As seen, the control throttle magnitude flips between 0 and 1 corresponding to positive and negative values of the switching parameter respectively.

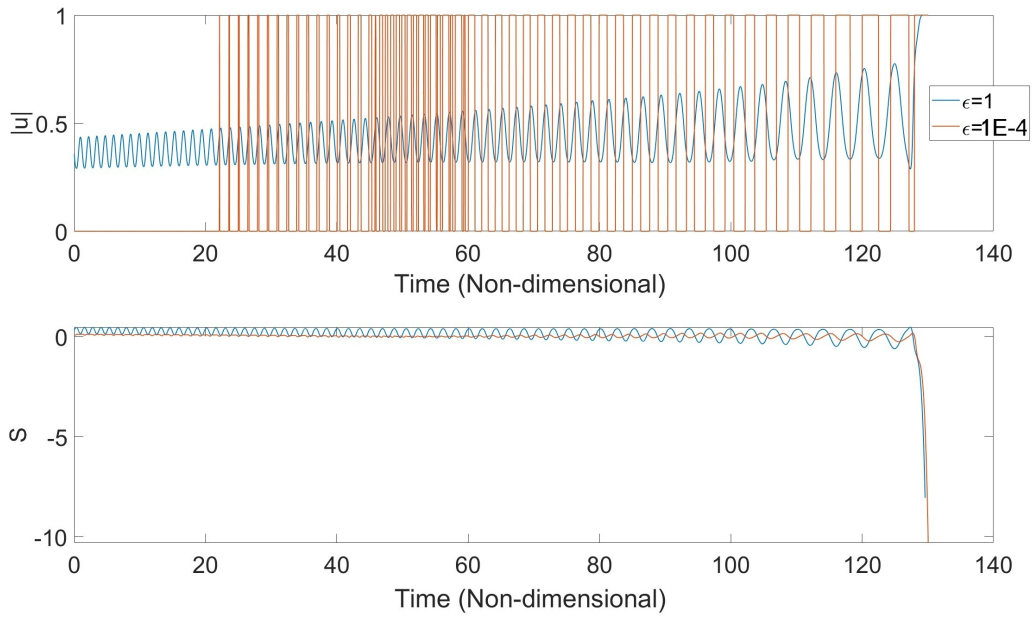

Figure 6.5: Control Smoothing for transfer to an L_1 halo orbit

Fig 6.6 demonstrates the relation between the spacecraft trajectory and the true anomaly of the spacecraft with respect to Saturn in the two body problem. A large portion of the initial spiral trajectory is spent coasting. The thrust arcs initially occur near periapsis regions, in order to raise the apoapsis. However, soon after, thrust arcs begin occurring at apoapsis and coast arcs near periapsis in order to raise the periapsis. The development of this large initial coast arc is an interesting feature, the reason for which is potentially the initial guess utilized. Fig 6.7 depicts the evolution of the control throttle magnitude for different values of ϵ. As we can see, the converged transfer with smoothed control (ϵ=1) possesses a control throttle magnitude of less than 0.5 for approximately the first 20 non dimensional time units. Further, it can be seen that as ϵ reduces, the region which had the smoothed control throttle magnitude less than 0.5 converges down to a coast arc corresponding to $|u|$=0. Regions where the smoothed control possesses $|u| > 0.5$ evolves to a thrust arc when $\epsilon \to 0$.

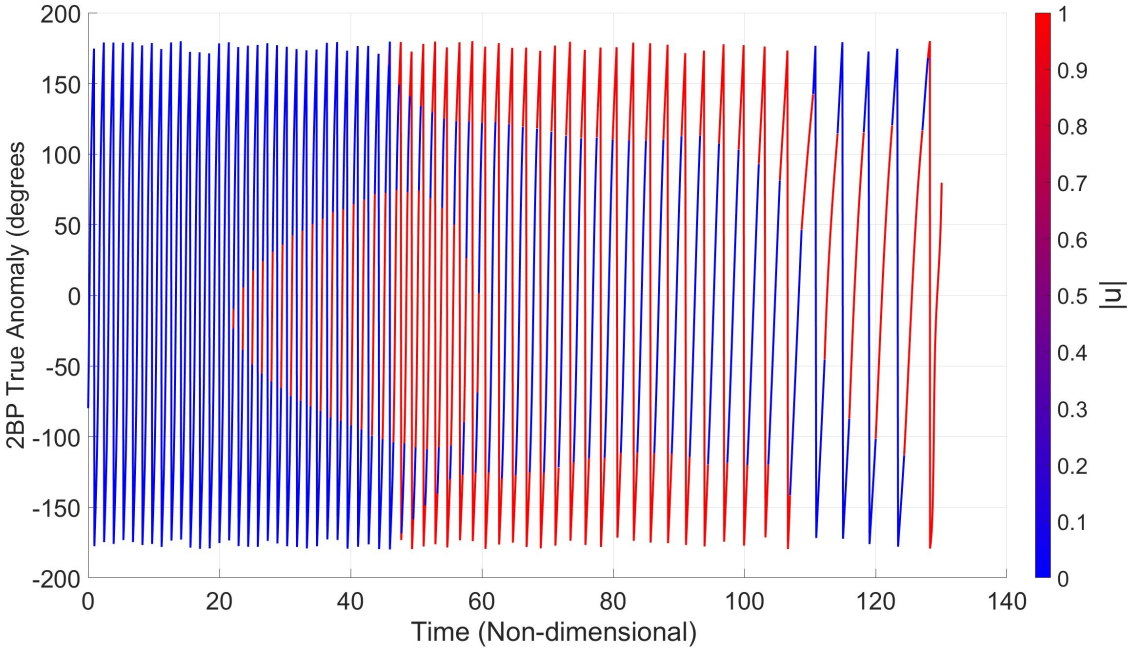

Figure 6.6: Relationship between apsis and thrusting arcs for transfer to an L_1 halo orbit

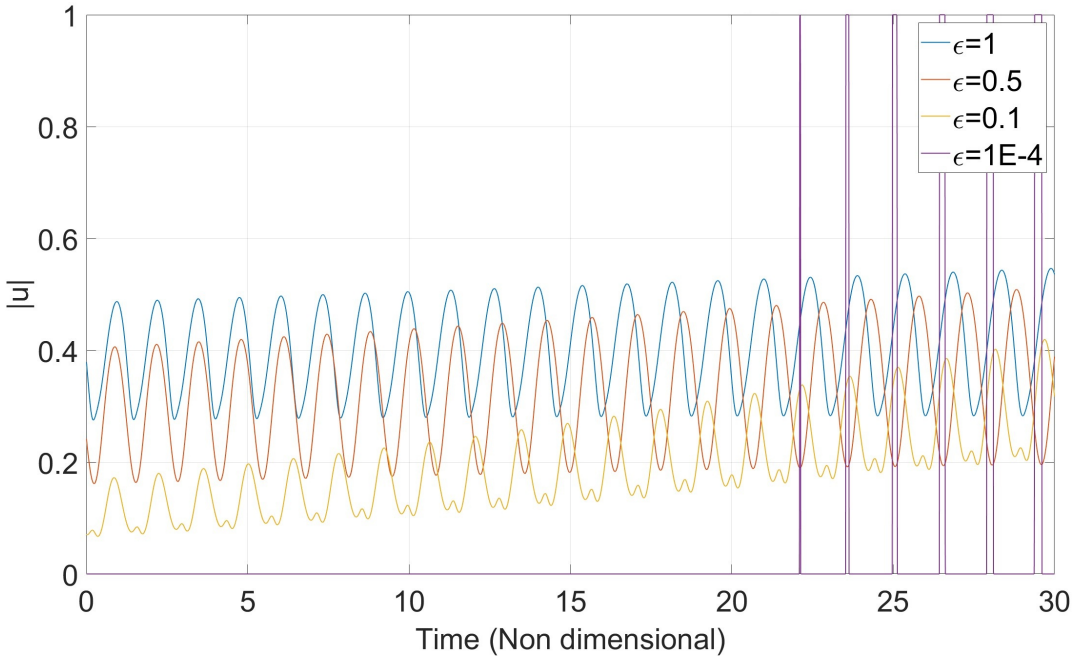

Figure 6.7: Halo orbit transfer control throttle magnitude for the first 100 days

In addition, the angle between the thrust vector and the velocity vector is an effective way to

evaluate the impact of the smoothing, as seen in Fig 6.8. Note that the discontinuous nature of the evolution of the angle for the bang-bang control profile case is due to the fact that by definition, the spacecraft undergoes thrust and coast regimes. As seen, with a smoothed control, the angle between the velocity and thrust vector is on average larger when compared with the angle for a bang-bang control profile solution. It is known that thrusting in the direction of the velocity is one of the most effective ways to change the Jacobi constant. Towards the end of the trajectory, the angle between the velocity and thrust vectors grows rather large. This is required for the final trajectory change in order to insert onto the target orbit. Fig 6.9 depicts the changing Jacobi constant. The stair-like structure is due to the bang-bang control profile, alternating between thrust and coast arcs. Interestingly, it can be seen from Fig 6.9 that the change in Jacobi constant appears to be highest during the time period of approximately 50-60 time units. Comparing this with Fig 6.5, we see that this period is also the region with the most significant flipping of the control throttle magnitude between 1 and 0. While the obtained transfer is propellant mass optimal, there may be more efficient transfers achievable depending on the initial guess utilized. This can also be seen in that initially, the trajectory utilizes a long coast arc. Other transfers may involve thrust arcs at the beginning for a faster transfer, while minimizing propellant usage.

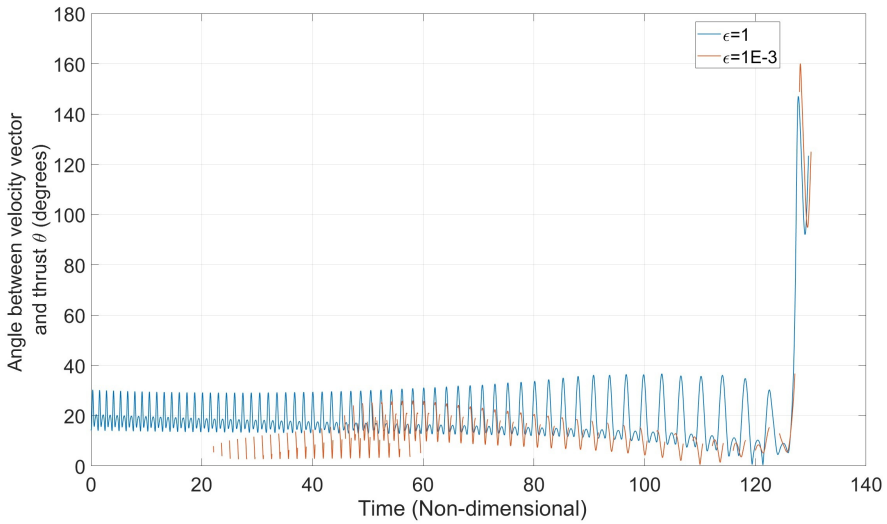

Figure 6.8: Impact of smoothing on angle between thrust and velocity vectors for transfer to an L_1 halo orbit

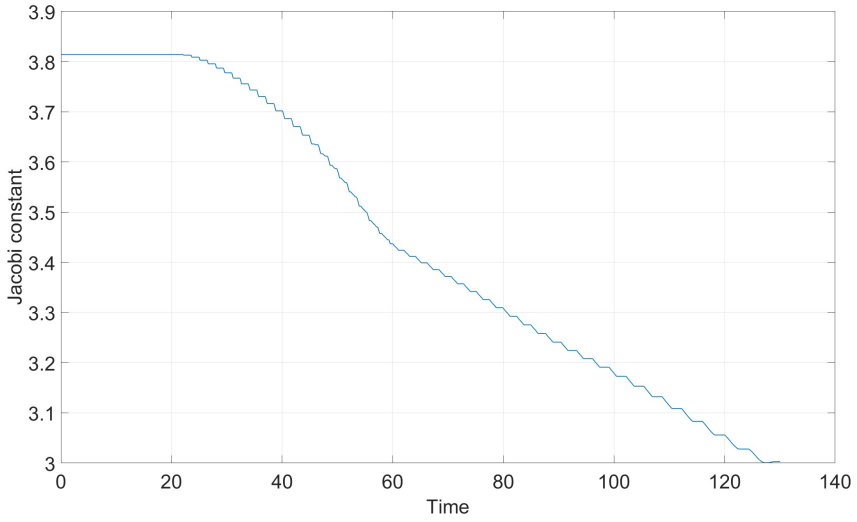

Figure 6.9: Jacobi Constant evolution for transfer to an L_1 halo orbit

It is important to note that the optimal control formulation defined in Chapter 4 is for an unconstrained time of flight problem. Thus, the transfer time of flight is free to vary during the continuations process. However, due to the nature of multiple shooting and natural parameter continuation, the solutions generated resemble each other. This can be seen in Fig 6.10.

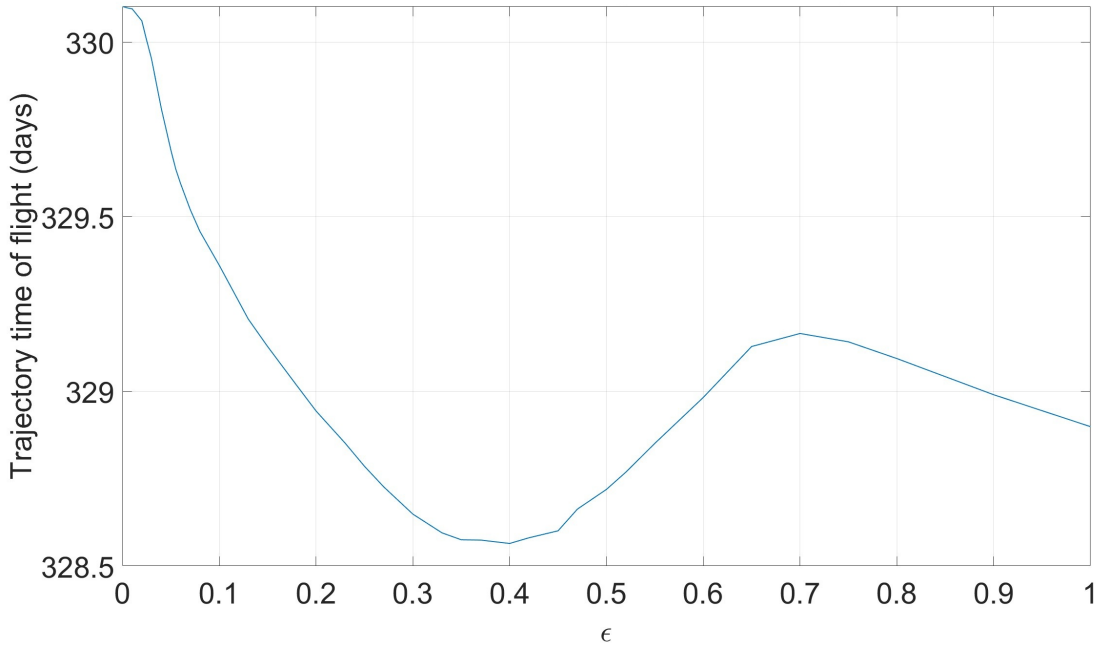

Figure 6.10: Effect of smoothing on time of flight for halo transfer

Similarly, as hard constraints are not enforced on the initial states, they are free to drift along the manifold described by the initial constraints defined. The evolution of some of the orbit elements at t_0 are seen in Figures 6.11, 6.12 and 6.13. Finally, the complete propellant optimal trajectory is plotted in the inertial frame in Fig 6.14.

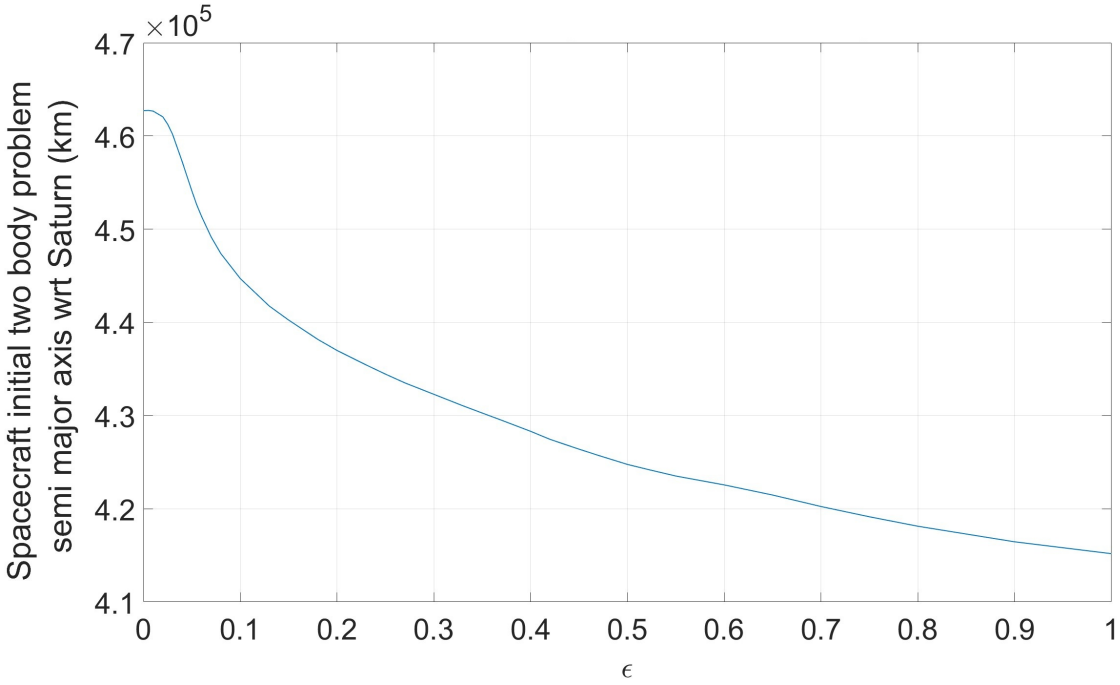

Figure 6.11: Effect of smoothing on initial semi major axis for halo transfers

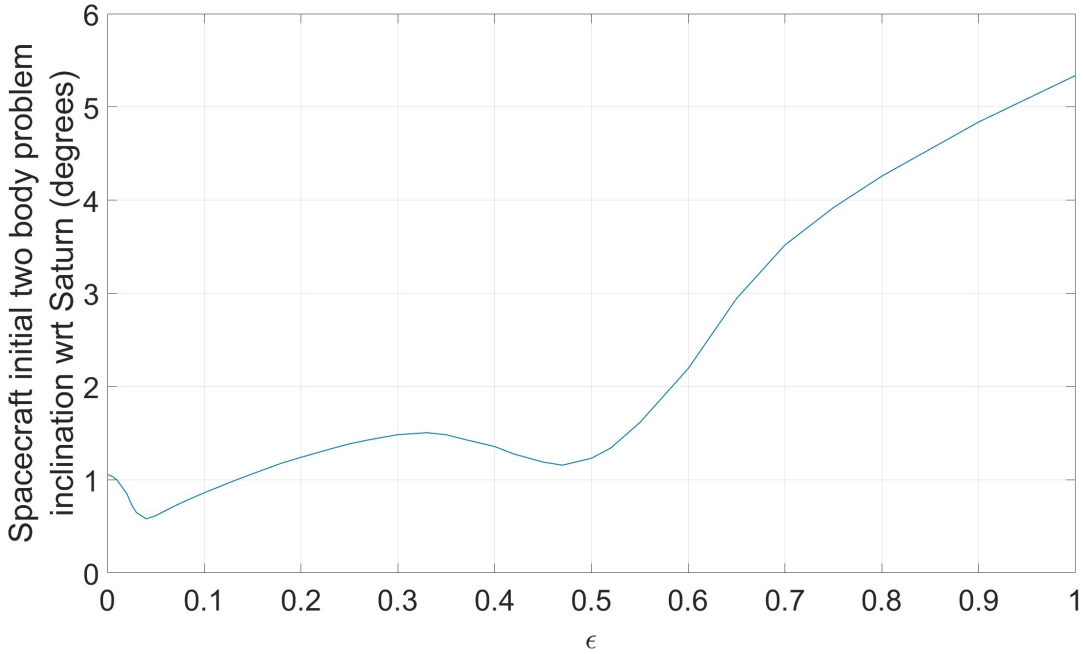

Figure 6.12: Effect of smoothing on initial inclination for halo transfers

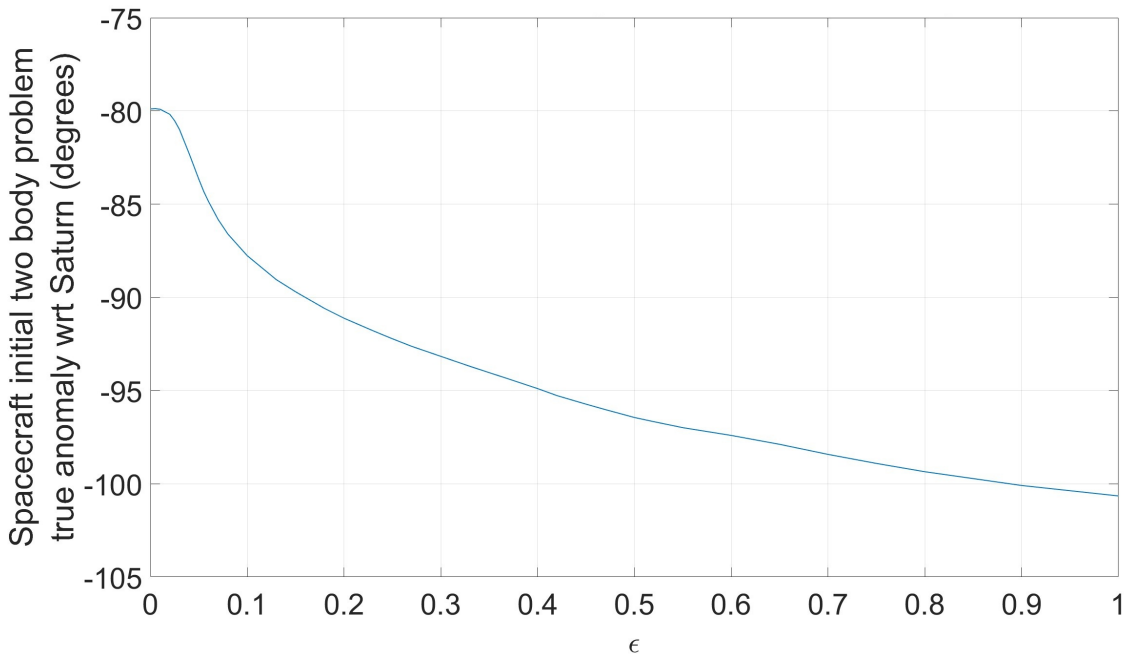

Figure 6.13: Effect of smoothing on initial true anomaly for halo transfers

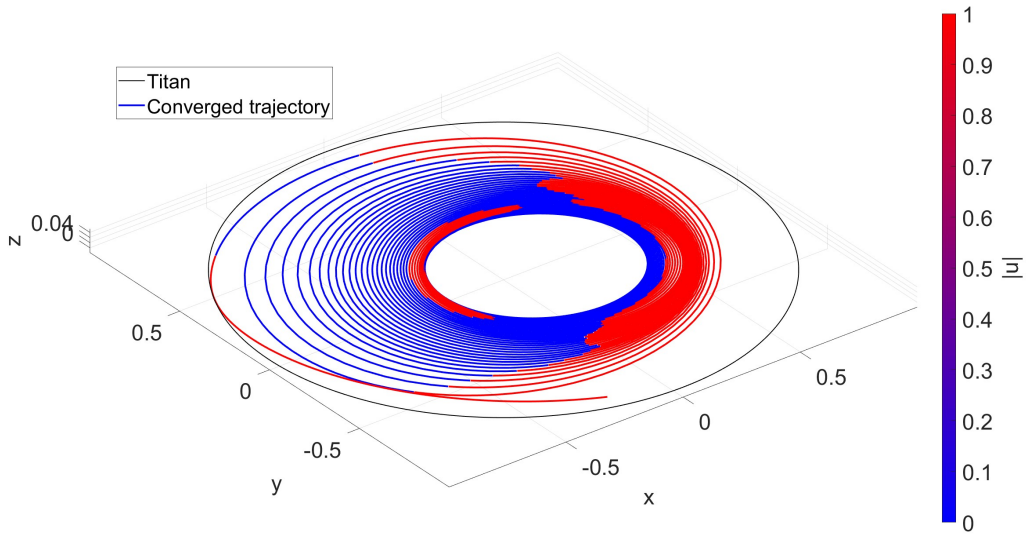

Figure 6.14: propellant mass optimal halo orbit transfer in the inertial frame

6.2 Transfer to an L_2 Vertical Orbit

The same initial guess used for the previous transfer is used to generate a propellant mass optimal transfer to an L_2 Vertical Orbit. Fig 6.15 depicts the Vertical orbit transfer with a smoothed control.

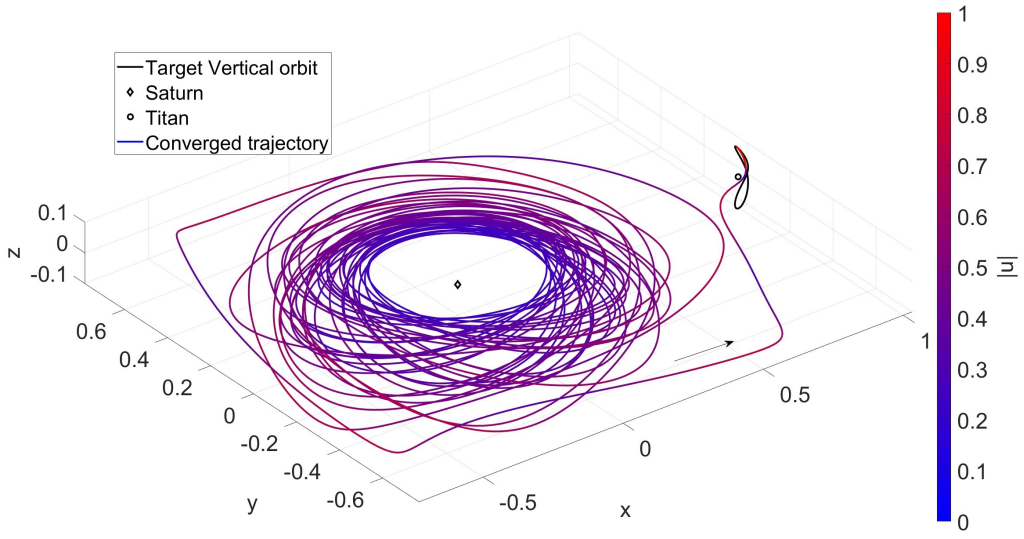

Figure 6.15: Converged vertical orbit transfer with smoothed control in the CR3BP rotating frame

Next, natural parameter continuation is used to generate a propellant mass optimal transfer, with the required bang-bang control profile as seen in Fig 6.16. A detailed view of the final segments of the transfer is shown in Fig 6.17. An important feature in the transfer to note is the close approach of the trajectory to Titan. As seen, this appears to deflect the trajectory slightly. The trajectory appears to utilize this effective gravity assist in order to change directions with a coast arc. Once the trajectory exits the immediate vicinity of the primary, thrusting begins again in order to make the final corrections to insert onto the vertical orbit. Although the final transfer effectively utilizes the flyby with Titan to change the trajectory, care must be taken with the corrections procedure. Close passes with primaries as seen here, can cause the corrections procedure to become extremely sensitive to parameter changes. Smaller steps must be taken in the

corrections procedure for trajectories requiring close passes to the primary.

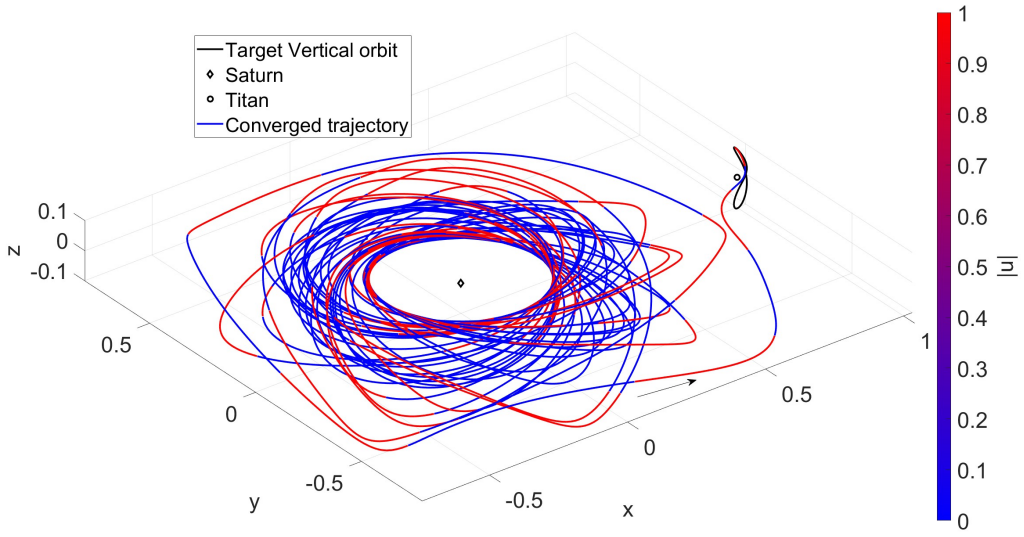

Figure 6.16: propellant mass optimal vertical orbit transfer in the CR3BP rotating frame

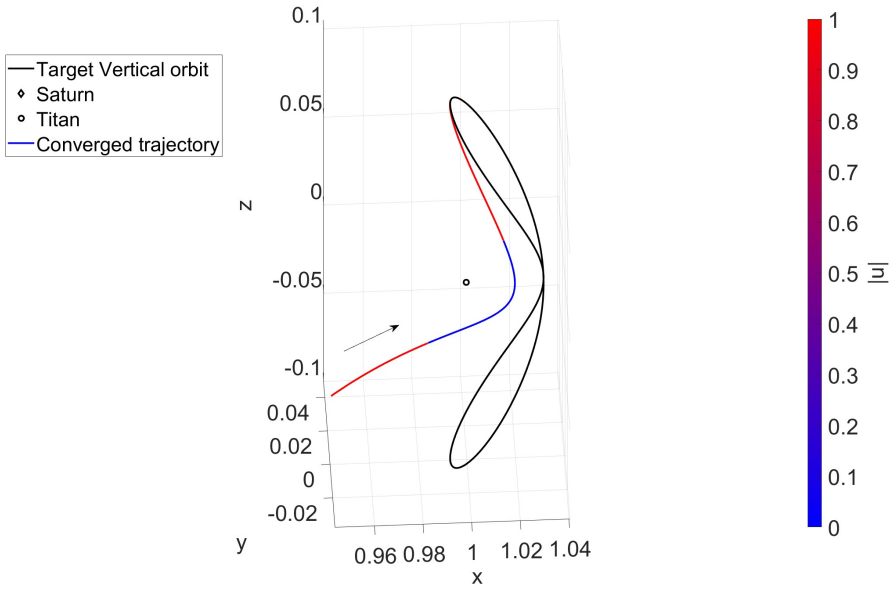

Figure 6.17: Zoomed in view of propellant mass optimal vertical orbit transfer in the CR3BP rotating frame

The impact of the variation of ϵ can be studied through the change in propellant requirements

as seen in Fig 6.18 and Table 6.1. As seen, there is a drastic improvement in the propellant requirements when comparing the smoothed control solution with the optimal bang-bang control profile solution, with a propellant requirement reduction of 89.7006797834071 kg.

ϵ	Propellant Usage (kg)
1	629.331739355071
0.9	625.182303548824
0.7	614.347448876537
0.5	597.876259563091
0.3	577.796693447913
0.1	555.778424301673
0.0001	539.631059571664

Table 6.2: Impact of ϵ on propellant usage for transfer to an L_2 vertical orbit

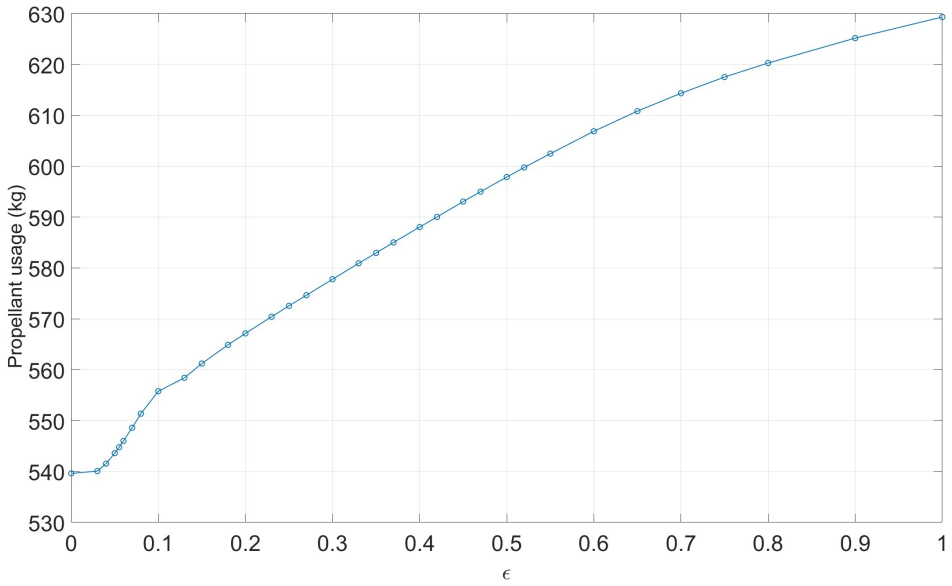

Figure 6.18: Effect of ϵ on propellant usage for transfer to an L_2 vertical orbit

Next, Fig 6.19 proves that reducing ϵ results in bang-bang control profiles. In addition, the relationship between the control throttle magnitude and the switching parameter S is verified.

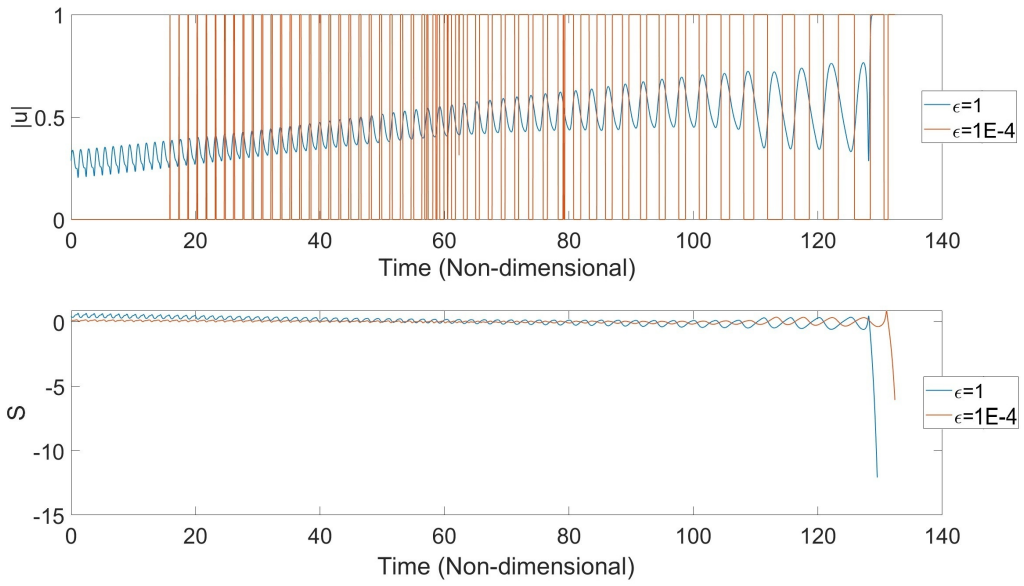

Figure 6.19: Control Smoothing for transfer to an L_2 vertical orbit

Fig 6.20 demonstrates the relation between the thrust arcs and the true anomaly in the two body problem, centered at Saturn. Similar to the previous transfer, a large portion of the initial spiral trajectory is spent coasting. The thrust arcs initially occur near periapsis regions, in order to raise the apoapsis. However, soon after, thrust arcs begin occurring at apoapsis and coast arcs near periapsis in order to raise the periapsis. When compared to the transfer to the halo orbit previously compared, while the overall structure of the coast and thrust arcs are similar, the transition from periapsis thrust to apoapsis thrust takes longer for the case of the vertical transfer. Similar to before, the existence of the large initial coast arc can be attributed to the specific initial guess used. This hypothesis is supported by the fact that all transfers computed in this thesis utilize the same initial planar trajectory guess. Fig 6.21 shows the control throttle magnitude for the first 100 days. Here, while the fully smoothed control throttle magnitude remains under 0.5 for a large amount of time, the bang-bang control case converges down to a coast arc much earlier than when the smothed throttle magnitude rises above 0.5.

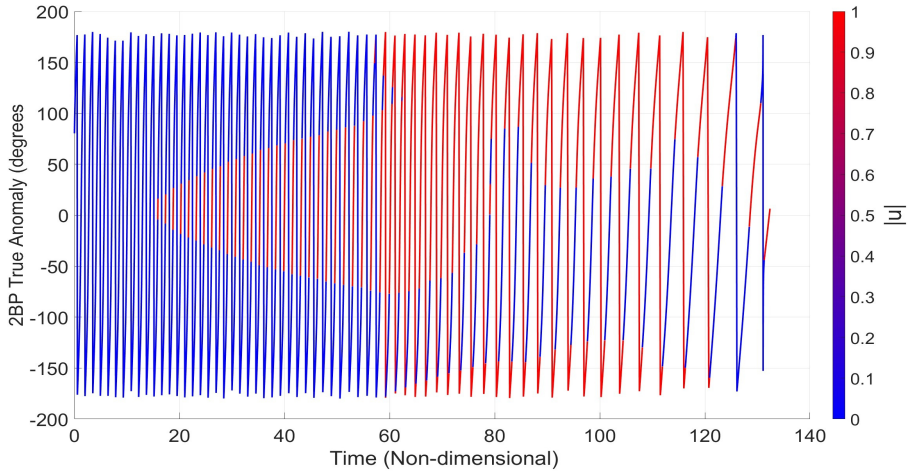

Figure 6.20: Thrust and coast arcs associated with periapsis and apoapsis regions for transfer to an L_2 vertical orbit

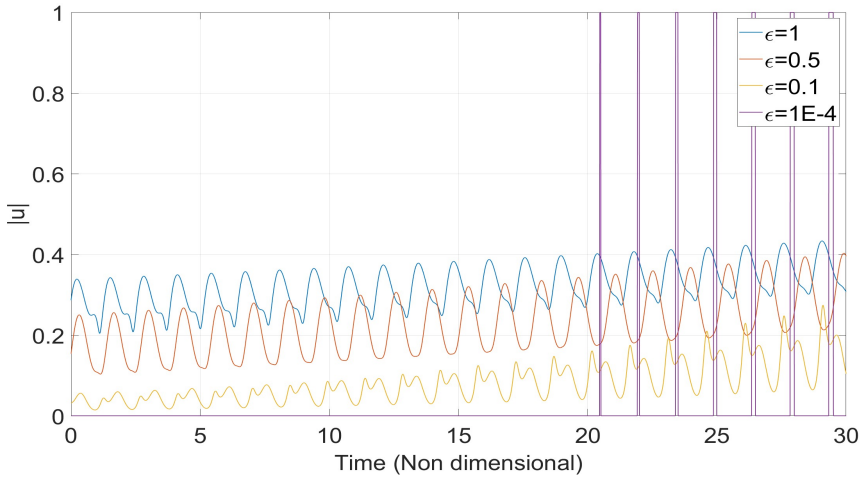

Figure 6.21: Vertical orbit transfer control throttle magnitude for the first 100 days

The impact of smoothing on the angle between the velocity and thrust vectors is dramatic, with the average angle for the smoothed control case being significantly higher than that of the propellant mass optimal case. However, the average angle for the propellant mass optimal case is higher than that of the propellant mass optimal halo orbit transfer.

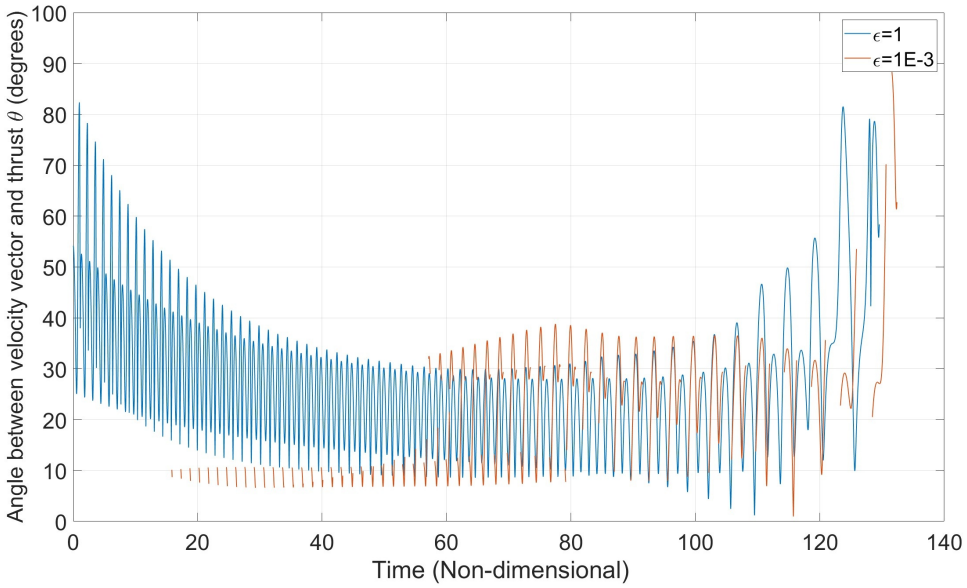

Figure 6.22: Evolution of angle between thrust and velocity vectors for transfers to an L_2 vertical orbit

The evolution of the Jacobi constant is depicted in Fig 6.23. The complete propellant mass optimal vertical orbit transfer is plotted in the inertial frame as seen in Fig 6.27. As described before, following a brief coast period, the spacecraft begins apoapsis raising thrust arcs before following with periapsis raising maneuvers. The final part of the trajectory involves a thrust arc to complete the insertion into the Vertical orbit. Figures 6.24, 6.25 and 6.26 show the impact of smoothing on the initial orbit elements

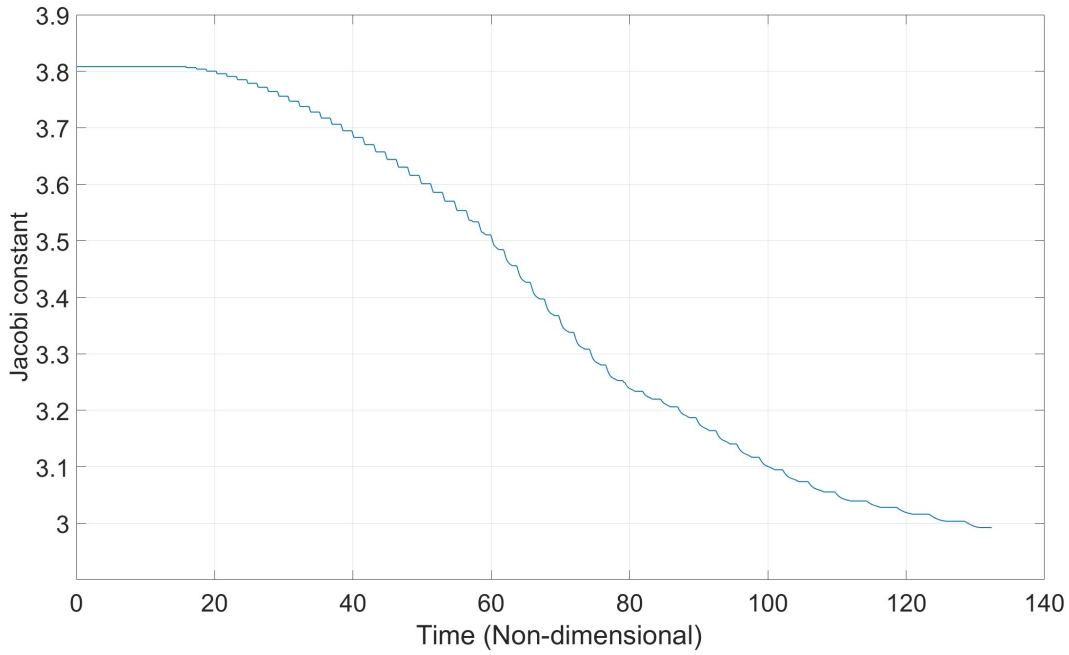

Figure 6.23: Evolution of Jacobi constant for propellant mass optimal vertical orbit transfer

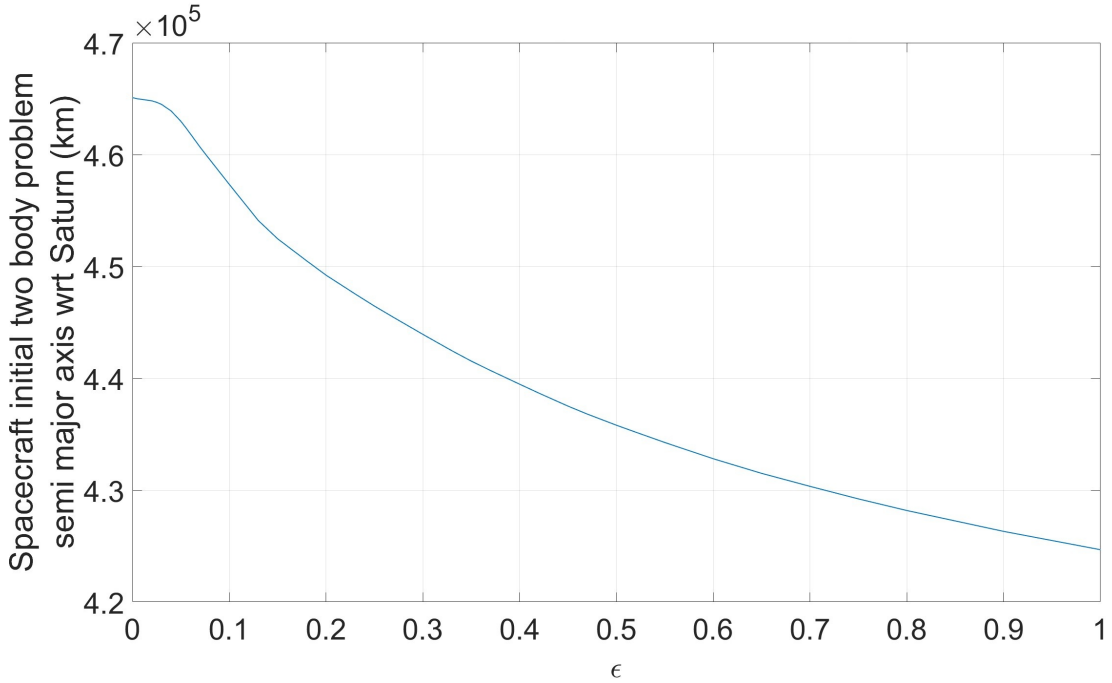

Figure 6.24: Effect of smoothing on initial semi major axis for vertical orbit transfers

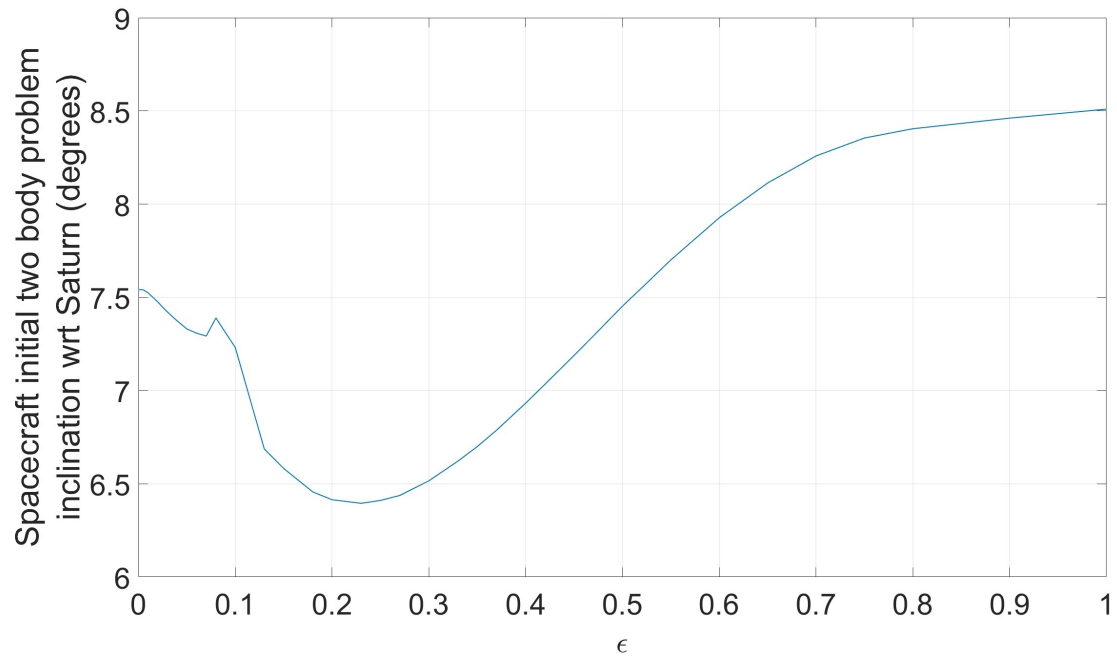

Figure 6.25: Effect of smoothing on initial semi major axis for vertical orbit transfers

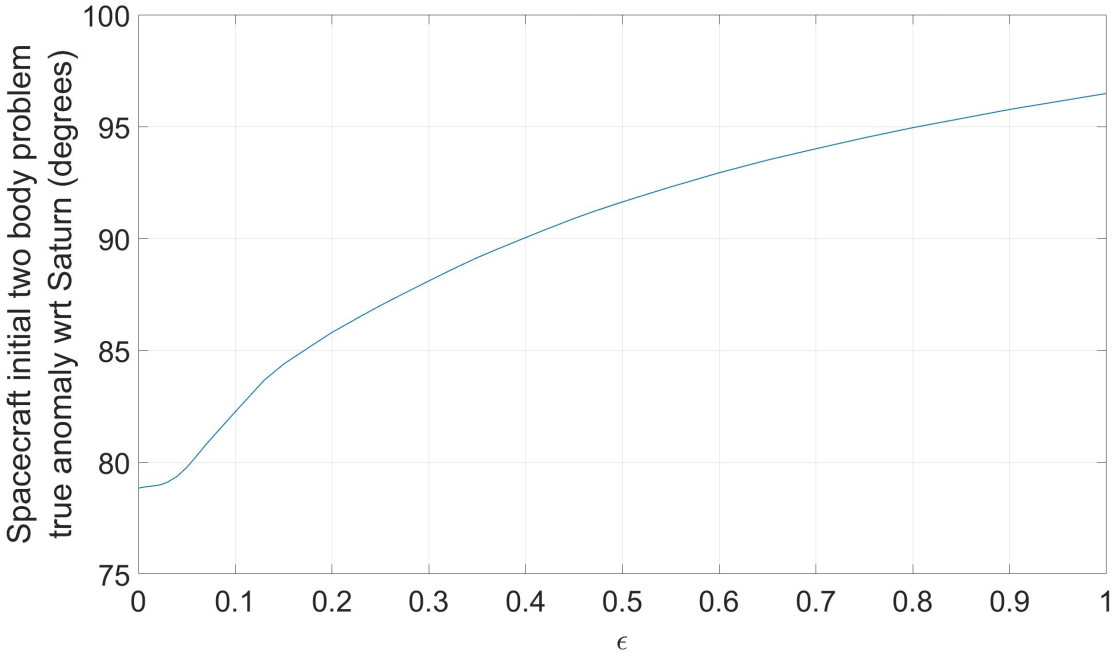

Figure 6.26: Effect of smoothing on initial semi major axis for vertical orbit transfers

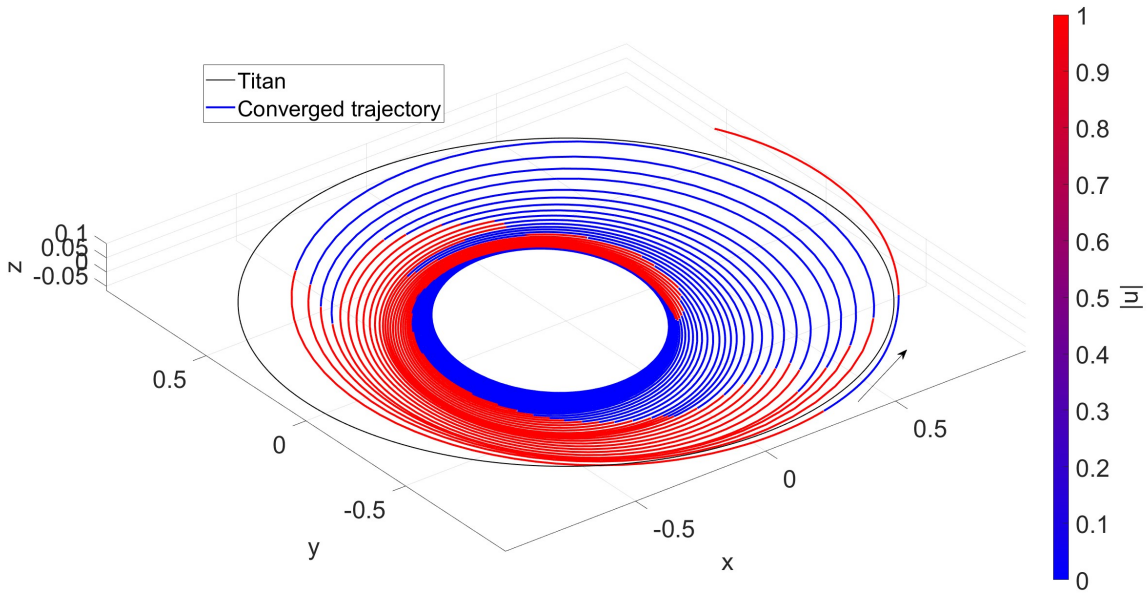

Figure 6.27: Propellant mass optimal vertical orbit transfer in the inertial frame

6.3 Family of Halo Orbit Transfers

Utilizing the final propellant mass optimal transfer to the selected halo orbit, propellant mass optimal transfers to other members of the family can be computed via continuation. The properties of the next halo orbits targeted are defined in Table 6.3 and the specific states targeted along each orbit are defined in Table 6.4. The chosen Halo orbits and the target states are shown in Fig 6.28

Orbit Number	Orbit Period (days)	Jacobi Constant	Closest approach to Titan (km)
1	5.04273266085836	3.00327905281339	7506.13535
2	4.78924739615392	3.00351226848146	5509.46596
3	4.53590397025445	3.00380177985883	3500.19857
4	4.40932848946008	3.0039654902571	2476.54186
5	4.35872837848503	3.00403393103537	2059.79639

Table 6.3: Properties of L_1 Halo orbits targeted

Orbit Number	x	y	z	$\dot{x}$	$\dot{y}$	$\dot{z}$
1	0.98547	0.021977	0.03563	0.03044	0.021753	-0.06592
2	0.98843	0.020432	0.032832	0.03036	0.01402	-0.07367
3	0.98962	0.017469	0.034374	0.027100	0.01403	-0.07263
4	0.99182	0.01639	0.03079	0.02703	0.00668	-0.08219
5	0.992189	0.015703	0.03082	0.02621	0.006225	-0.08280

Table 6.4: Target States along halo orbits

With a goal of studying the polar regions of Titan, NRHO orbits are of great importance of value. These are specific libration point orbits with close approaches to the polar regions of Titan, and are quite stable, with respect to their stability indices. However, attempting to converge to a propellant mass optimal transfer to the final halo orbit displayed, beginning with the planar initial guess is extremely difficult, and faces severe convergence issues. However, beginning from a propellant mass optimal transfer to an easier to reach orbit allows us to generate families of transfers to more favorable halo orbits. These orbits considered are shown in Fig 6.28. The NRHO is the final orbit in the Figure - the pale blue orbit. The properties of the final propellant mass optimal transfers to the various halo orbits are shown in Table 6.5. As seen, the closer the target orbits get to an NRHO, the more propellant is required. This can be attributed to the stable nature

of NRHO orbits.

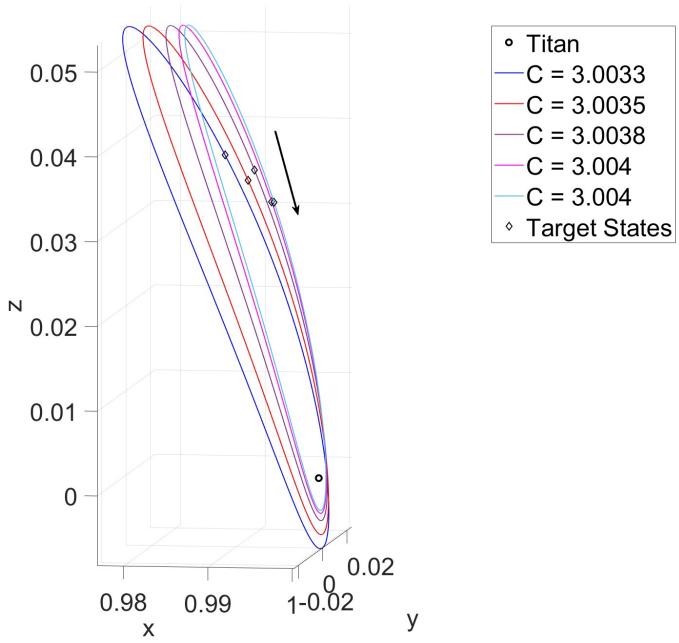

Figure 6.28: L_1 Halo orbits and associated target states

Orbit Number	Total Jacobi change	Propellant Usage (kg)	Time of flight (days)
1	0.810738	515.659089	330.1011
2	0.81576	526.8707516	330.1874
3	0.81829	543.9189895	330.2913
4	0.816927	549.030499	330.6026
5	0.843714	562.628055	331.0454

Table 6.5: Details of propellant mass optimal transfers to family of L_1 Halo orbits

The propellant mass optimal transfers targeting different halo orbits are seen in Figures 6.29, 6.30 and 6.31. Due to the nature of the continuation procedure, the transfers greatly resemble the transfer to the initial halo orbit. A comparison between the trajectory geometry is shown in Fig 6.32, between the transfers to the first and fifth halo orbits. Here, it is easier to see that, although the transfers are extremely similar, there are differences in the timing of certain sections. As seen, with the first transfer, the final direction change occurs closer to x=0 while the same change occurs in the next transfer near x=0.6.

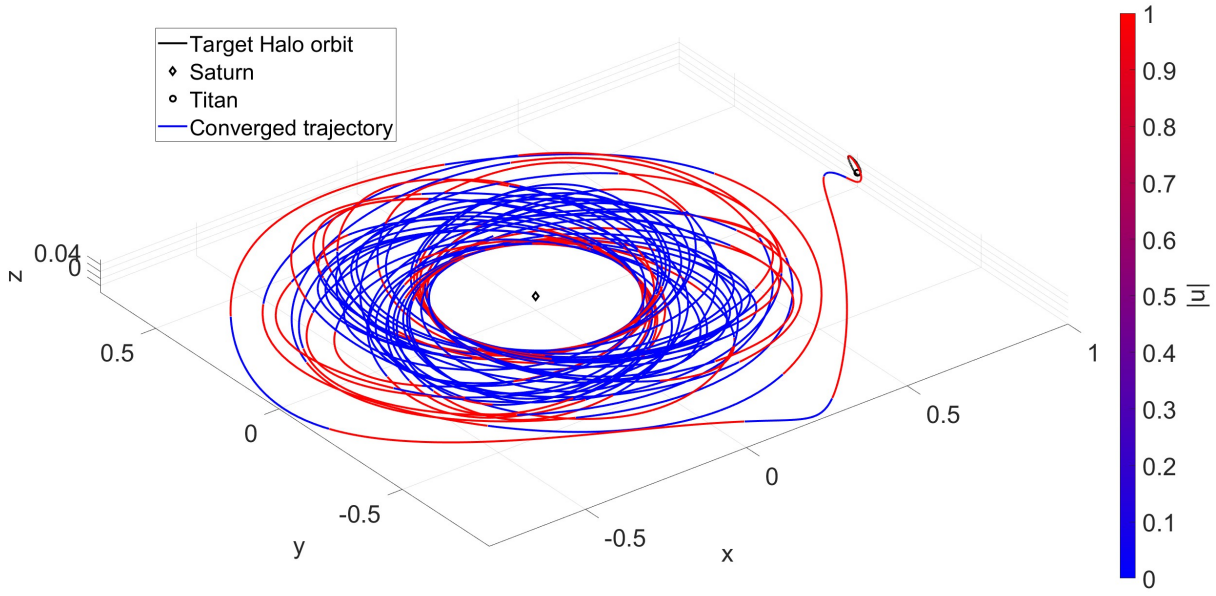

Figure 6.29: Propellant mass optimal transfer to halo orbit 2

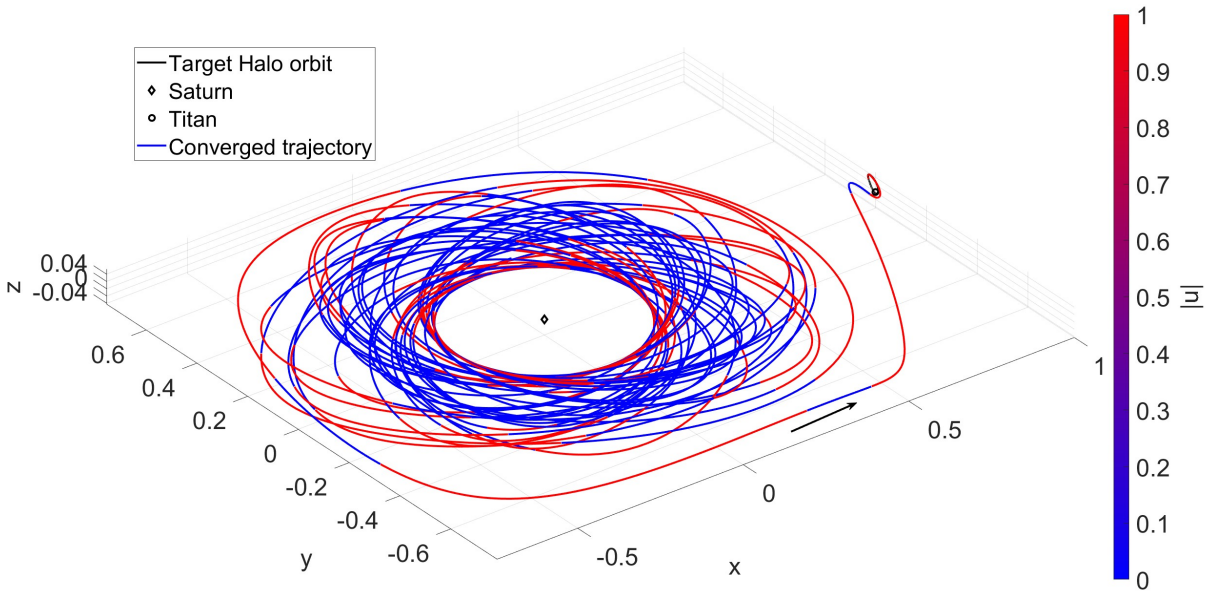

Figure 6.30: Propellant mass optimal transfer to halo orbit 4

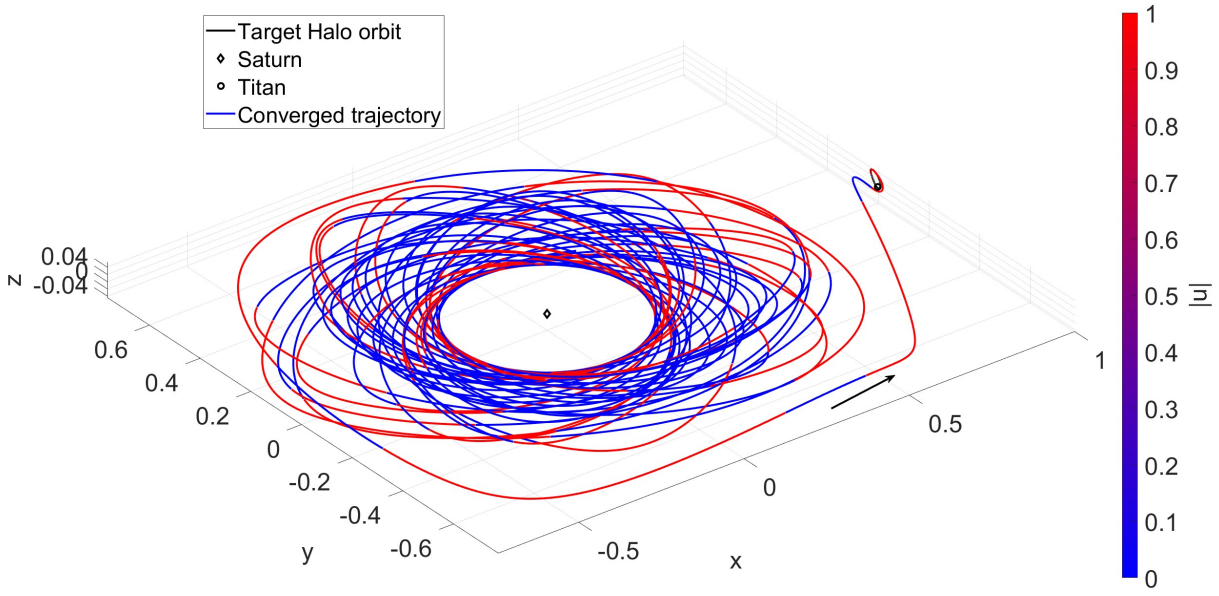

Figure 6.31: Propellant mass optimal transfer to halo orbit 5

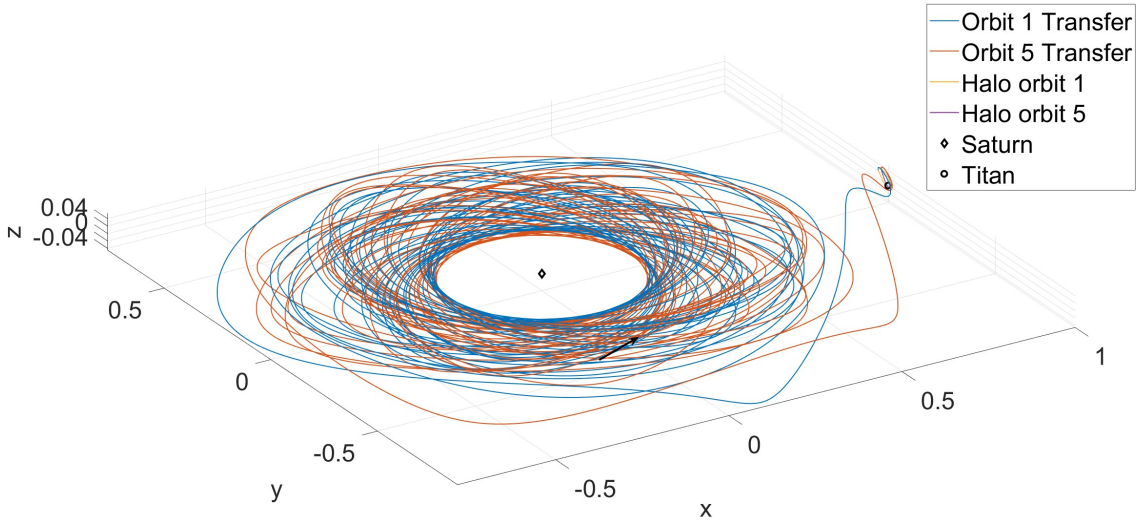

Figure 6.32: Geometry comparison between transfers to different halo orbits

Chapter 7

Conclusion

7.1 Summary

Primer vector theory has been used to generate propellant mass optimal transfers in the Saturn-Titan CR3BP dynamical model, using a low thrust propulsive system. The transfers targeted libration point orbits in the vicinity of Titan, characterized by close passes to the polar regions of Titan and possessing favorable views of the polar regions for a large part of the orbit to aid in future missions to study the liquid methane lakes of Titan. A procedure to generate an initial guess was developed, and combined with multiple shooting and natural parameter continuation to converge to the desired optimal transfer. The detailed approach is applied to compute a propellant mass optimal transfer to an L_2 vertical orbit as well as an L_1 halo orbit. The resultant trajectories are analyzed and the effect of the optimization procedure in discussed. Next, the halo orbit transfer is further used to generate transfers to a nearby NRHO orbit for improved polar coverage.

7.2 Future Work

- A key assumption of this work is that the initial state is constrained with respect to the eccentricity and distance from Saturn. Enforcing hard constraints on the spacecraft initial position and velocity states would be ideal. However, the inclusion of hard constraints complicates the convergence process, and introduces sensitivities into the corrections procedure.

- The approach used to generate an initial guess trajectory is suitable for generating trajectories that do not need to cross primaries. As seen, when targeting L_2 orbits, a gravitational assist is necessarily involved and introduces sensitives into the procedures. Regularization would be an effective method of avoiding this sensitivity, in order to transition to trajectories passing the primary.

- The gravitational effects of Saturn's other moons could be incorporated to generate a higher fidelity transfer, perhaps utilizing continuation based on a mass parameters, transitioning from the defined CR3BP model to an n body model.

Bibliography

[1] R. Broucke. Stability of periodic orbits in the elliptic, restricted three-body problem. AIAA Journal, 7:1003–1009, 1969.

[2] Franco Bernelli-Zazzera Chen Zhang, Francesco Topputo and Yu-Shan Zhao. Low-thrust minimum-fuel optimization in the circular restricted three-body problem. Journal of Guidance, Control, and Dynamics, 38:1501–1510, 2015.

[3] Bruce A. Conway. Spacecraft Trajectory Optimization. Cambridge University Press, 2010.

[4] Manuel Sanjurjo Rivo David Morante and Manuel Soler. A survey on low-thrust trajectory optimization approaches. Aerospace, 8, 2021.

[5] Randy Paffenroth-H. Keller Donald Dichmann J Galán Eusebius Doedel, V Romanov and Andre Vanderbauwhede. Elemental periodic orbits associated with the libration points in the circular restricted 3-body problem. International Journal of Bifurcation and Chaos, 2007.

[6] Natasha Bosanac Jeffrey R. Stuart Ian Eliott, Christopher Sullivan Jr. and Farah Alibay. Designing low-thrust trajectories for a smallsat mission to sun–earth l5. Journal of Guidance, Control, and Dynamics, 43:1854–1864, 2020.

[7] José J. Guzmán James M. Longuski and John E. Prussing. Optimal Control with Aerospace Applications. Springer, 2014.

[8] D.F. Lawden. Optimal Trajectories For Space Navigation. Butterworths, 1963.

[9] Ali H. Nayfeh and Balakumar Balachandran. Applied Nonlinear Dynamics: Analytical, Computational, and Experimental Methods. Wiley, 1995.

[10] Kenshiro Oguri and Jay W. McMahon. Stochastic primer vector for robust low-thrust trajectory design under uncertainty. Journal of Guidance, Control, and Dynamics, 45:84–102, 2022.

[11] Jeffrey S. Parker and Rodney L. Anderson. Low-Energy Lunar Trajectory Design. Wiley, 2014.

[12] Anastassios Petropoulos and Ryan Russell. Low-thrust transfers using primer vector theory and a second-order penalty method. AIAA/AAS Astrodynamics Specialist Conference and Exhibit, 2008.

[13] Antonios Tsourdos Senchun Chai Runqi Chai, Al Savvaris and Yuanqing Xia. A review of optimization techniques in spacecraft flight trajectory design. Progresses in Aerospace Sciences, 109, 2019.

[14] Ryan P. Russel. Primer vector theory applied to global low-thrust trade studies. Journal of Guidance, Control, and Dynamics, 30:460–472, 2007.

[15] Hanspeter Schaub and John Jenkins. Analytical Mechanics of Space Systems Fourth Edition. American Institute of Aeronautics and Astronautics, 2018.

[16] Daniel J. Scheeres. Orbital Motion in Strongly Perturbed Environments. Springer, 2012.

[17] Yanis Sidhoum and Kenshiro Oguri. Low-thrust trajectory optimization for enceladus exploration using indirect forward-backward shooting.

[18] Yanis Sidhoum and Kenshiro Oguri. On the performance of different smoothing methods for indirect low-thrust trajectory optimization. The Journal of the Astronautical Sciences, 70, 2023.

[19] John Snyder and Richard Hofer. Throttled performance of the spt-140 hall thruster. 50th AIAA/ASME/SAE/ASEE Joint Propulsion Conference 2014, 2014.

[20] V. Szebehely. The Theory of Orbits The Restricted Problem of Three Bodies. Academic Press, New Haven, CT, 1967.

[21] Ehsan Taheri and John L. Junkins. Generic smoothing for optimal bang-off-bang spacecraft maneuvers. Journal of Guidance, Control, and Dynamics, 41(11):2470–2475, 2018.

[22] Ehsan Taheri and John L. Junkins. Exploration of alternative state vector choices for low-thrust trajectory optimization. Journal of Guidance, Control, and Dynamics, 42(1):47–64, 2019.

[23] David A. Vallado. Fundamentals of Astrodynamics and Applications. Microcosm Press, 4th edition, 2013.